AMAS COURSE ON RANDOM MATERIAL MICROSTRUCTURES
RMM'04 – (PP.223–281) – WARSAW, FEBRUARY 2-4, 2004

Statistics of the structure and properties of inhomogeneous materials

M.T. TODINOV

Cranfield University
Reliability Engineering and Risk Management Centre, SIMS
Building 56b, Cranfield, Bedford, MK43 0AL, UK
m.t.todinov@cranfield.ac.uk

Variability of material properties is often attributable to inhomogeneity of the microstructure. Many materials are inhomogeneous, for example ferrous and non-ferrous alloys, composites, ceramics, plastics and biological materials. Determining the probability bounds on the variation of properties due to inhomogeneity is an important issue for structural integrity assessments.
The influence of the microstructural inhomogeneity is particularly strong for fracture properties as compared to other properties (e.g., the material's moduli). The reason, is that the fracture criteria are particularly sensitive to microstructural heterogeneities which lead to local zones of weak resistance to crack extension. Often, ahead of crack fronts in composite materials or in materials containing defects, the number density of the defects varies locally which is another manifestation of the microstructural inhomogeneity. Depending on the microstructural constituents or the local number density of the defects ahead of the crack front, the local fracture toughness varies widely. As a result, the uncertainty (variability) of properties associated with inhomogeneous structures is intrinsic. It is not due for example to a measurement imprecision or inability to control the experiment and therefore cannot be reduced or eliminated.
The statistics of structure and properties of inhomogeneous materials is an interplay of Materials Science and Applied Statistics. The intersections defined by the key words 'Statistics', 'Structure' and 'Properties', determine key research directions as shown in Fig. 1.

1. Statistics of random flaws in one-dimensional components

1.1. Introduction

In many industries, a strong emphasis is increasingly placed on reliability requirements which eliminate early-life failures (e.g. the offshore, aerospace and automotive industry). The early-life failures are often the result of poor manufacturing and inadequate design. A substantial proportion of the early-

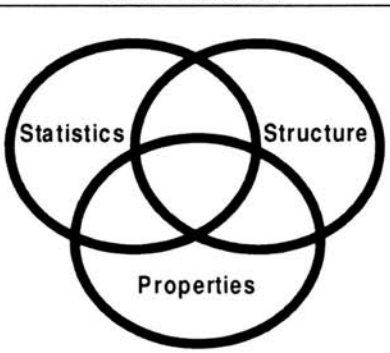

FIGURE 1. *Statistics and Structure*, *Statistics and Properties* and *Structure and Properties*. An important topic from the research direction 'Statistics and Structure' is the spatial statistics of flaws in one-dimensional components and the spatial statistics of duplex structures.

life failures are also due to variation of the *strength* which is a complex function of the *material properties*, *design configuration* and *dimensions*. An important factor affecting the strength of fibres and wires in particular, is the presence of flaws due to processing or manufacturing. The homogeneous Poisson process (Ross, 2000; Thompson, 1988) is often used as a statistical model for random flaws. Its main characteristics are: (i) the numbers of flaws in non-overlapping intervals are statistically independent; (ii) the probability of a flaw in intervals of the same length is the same. It depends only on the length of the interval, not on its location along the fibre/wire; (iii) the probability of more than one flaw in a very small interval is negligible. For random flaws following a homogeneous Poisson process with constant density $\lambda = \text{const}$ the cumulative distribution function of the distances x between adjacent flaws is given by the exponential distribution function $F(x) = 1 - e^{-\lambda x}$.

1.2. Specifying the upper bound of the flaw number density to guarantee a probability of failure initiated by defects below a maximum acceptable level

Each flaw (defect) is associated with a probability of initiating failure at a particular stress level [66]. The type of the flaws has a strong influence on the probability of failure initiation. Due to tensile tessellation stresses for example, alumina or silicon-based inclusions in steel wire are more likely to become initiators of failure compared to sulphide inclusions of the same diameter and numbers. In another example, sharp crack-like defects are characterised by a larger probability of triggering fracture compared to blunt defects. Furthermore, crack-like defects with a plane perpendicular to the

direction of the acting stress are more likely to initiate failure than cracks oriented along the direction of the acting stress. Consequently, an important problem is determining the maximum acceptable flaw density (the flaw density envelope) which limits the probability of triggering of failure by the flaws.

Suppose that a piece of length L, which has been cut from wire containing flaws with number density λ, is stressed to a tensile stress σ. It is assumed that flaws from a single type exist which follow a homogeneous Poisson process in the length L and, each of the flaws is characterised by a probability $F(\sigma)$ of initiating failure at the stress level σ.

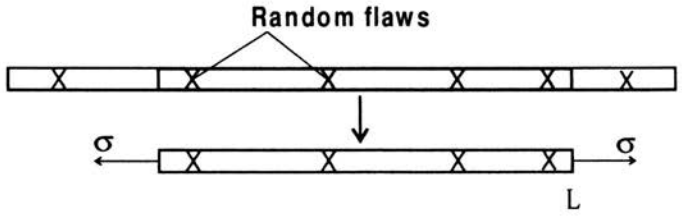

FIGURE 2.

The probability of initiating failure at a stress level σ by any of the flaws can be determined by subtracting from unity the probability of the complementary event that no failure will be initiated by the flaws. The probability $p^0_{(r)}$ of the compound event: 'exactly r flaws exist in the length L and none of them initiates failure at the stress level σ' is given by:

$$p^0_{(r)} = \frac{(\lambda L)^r e^{-\lambda L}}{r!}[1 - F(\sigma)]^r, \tag{1.1}$$

where λ denotes the flaw number density. This probability is a product of the probabilities of two independent events: (i) exactly r flaws reside in the piece of length L, the probability of which is given by the Poisson distribution $(\lambda L)^r \exp(-\lambda L)/r!$ and (ii) the event that none of the r flaws will initiate failure, the probability of which is given by $[1-F(\sigma)]^r$. The event 'no failure will be initiated at a stress level σ' is a union of the disjoint events $p^0_{(r)}$ and its probability p^0 is a sum of the probabilities defined by Eq. (1.1):

$$p^0 = \sum_{r=0}^{\infty} p^0_{(r)} = \sum_{r=0}^{\infty} \frac{(\lambda L)^r \exp(-\lambda L)}{r!}[1 - F(\sigma)]^r, \tag{1.2}$$

which can be simplified to

$$p^0 = \mathrm{e}^{-\lambda L} \sum_{r=0}^{\infty} \frac{[\lambda L\,(1 - F(\sigma))]^r}{r!} = \mathrm{e}^{-\lambda L}\mathrm{e}^{\lambda L[1-F(\sigma)]} = \mathrm{e}^{-\lambda L F(\sigma)}, \tag{1.3}$$

and the probability p_σ of triggering failure at a stress level σ becomes

$$p_\sigma = 1 - p^0 = 1 - \mathrm{e}^{-\lambda L F(\sigma)}. \tag{1.4}$$

By solving Eq. (1.4) numerically regarding λ (given a specified maximum acceptable probability of failure $p_{\sigma\,\max}$ at a stress level σ, the upper bound (the flaw density envelope) λ^*_σ can be determined:

$$\lambda^*_\sigma = -\frac{1}{LF(\sigma)} \ln(1 - p_{\sigma\,\max}). \tag{1.5}$$

The flaw density envelope guarantees that whenever the flaw number density λ is within it ($\lambda \leq \lambda^*_\sigma$) the probability of triggering failure is smaller than $p_{\sigma\,\max}$.

Figure 3 gives the dependence of the flaw number density envelope λ^*_σ from $p_{\sigma\,\max}$ for different values of $LF(\sigma)$ in case of 'weak' flaws ($F(\sigma) \approx 1$). In the vicinity of $p_{\sigma\,\max} = 0$, the dependencies can be approximated by straight lines with slopes equal to $1/L$. Equation (1.4) can also be rewritten in the following way:

$$p_\sigma = 1 - \mathrm{e}^{-\lambda' L}, \tag{1.6}$$

where $\lambda' = \lambda F(\sigma)$. Equation (1.6) provides a convenient formalism interpreting flaws with a number density λ, initiating failure with probability $F(\sigma)$

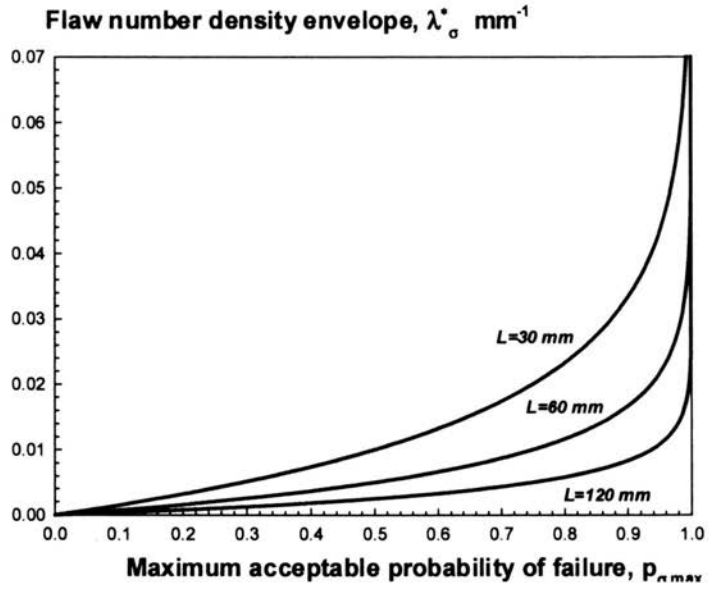

FIGURE 3.

as 'critical' flaws with number density $\lambda' = \lambda F(\sigma)$ initiating failure with certainty ($F(\sigma) = 1$). According to this formalism, the probability of no failure is simply equal to the probability that a critical flaw will not be present in the piece of length L. The product $\lambda' = \lambda F(\sigma)$ is an important invariant associated with materials containing flaws. The same probability of failure at a stress level σ can characterise two components one of which has a high density of flaws which trigger failure with small probability and the other is characterised by a low density of flaws which trigger fracture with high probability. The condition is the product (invariant) $\lambda' = \lambda F(\sigma)$ characterising the components to be the same.

Equation (1.5) specifies the flaw number density envelope necessary to guarantee with a specified probability no failure initiated by flaws. For weak flaws (e.g. carbides in steels) which trigger cleavage easily at the stress level σ, the probability of triggering failure at the stress level σ can be assumed to be approximately unity $F(\sigma) \approx 1$. In this case, the probability of failure of the loaded length L becomes equal to the probability that at least one flaw will be present in the length L: $p_\sigma = 1 - \exp(-\lambda L)$. In the general case however, the probability $F(\sigma)$ of triggering failure from individual flaws will be a number between zero and unity. It can for example be determined theoretically, using fracture mechanics criteria (Ewalds and Wanhill, 1989)) or empirically, from tests at a specified stress level. Suppose that N tests have been conducted at a stress level σ involving multiple pieces of length L cut from wire (fibre) with known flaw number density λ. If N_f is the number of failures caused by flaws, the probability $F(\sigma)$ of triggering failure by the flaws can be determined by solving $N_f/N = 1 - \exp(-\lambda L F(\sigma))$ with respect to $F(\sigma)$.

It must be pointed out that Eq. (1.4) can be generalised for a 3D or 2D components. In the three-dimensional case the equation becomes:

$$p_\sigma = 1 - p^0 = 1 - \mathrm{e}^{-\lambda V F(\sigma)}, \tag{1.7}$$

where V is the volume subjected to a stress σ and λ is the number density of the defects (per unit volume). From Eq. (1.7), it follows that the smaller the stressed volume V is the smaller is the probability of failure. Equation (1.7) for example, provides one of the reasons why between two strings of different length, from the same material, the longer string is less reliable.

1.3. Clustering of flaws following a homogeneous Poisson process in wires and fibres of finite length

Often, in thin fibres and wires, a configuration where two or more flaws are closer than a critical distance s cannot be tolerated during loading be-

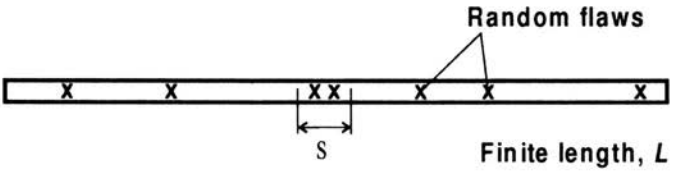

FIGURE 4.

cause clusters of two or more flaws within a critical distance act as single larger flaw. Clustering of two defects (flaws) within a critical distance s decreases dangerously the load-bearing cross section and is associated with a substantial stress concentration which decreases the load-bearing capacity. As a result, the probability of failure during loading is strongly correlated with the probability of clustering of flaws over a critical small distance s (Figure 4).

For a piece of length L, cut from wire containing defects following a homogeneous Poisson process, where the number of defects n is known over the length L, the successive coordinates of the n defects are uniformly distributed over the length L. This is a well-known property of the homogeneous Poisson process, discussed for example in (Ross, 2000; Thompson, 1988). For the case related to a known number of flaws in wire of length L, the equation

$$P = \left(1 - \frac{1}{L}\sum_{i=1}^{n-1} s_{i,i+1}\right)^n \tag{1.8}$$

has been derived in [58] for the probability P of existence of gaps greater than specified minimum gaps $s_{i,i+1}$ between adjacent uniformly distributed flaws in the finite length L. For four specified minimum gaps s_{12}, s_{23}, s_{56}, and s_{67} between four pairs of adjacent flaws, according to Eq. (1.8) the probability that the minimum specified gaps will exist is given by

$$P = \left(1 - \frac{s_{12} + s_{23} + s_{56} + s_{67}}{L}\right)^9, \tag{1.9}$$

where $n = 9$ is the number of flaws.

Indeed, suppose that nine flaws are uniformly distributed in a one-dimensional component with length L

Assume that the locations of the flaws are 'generated' to be uniformly distributed along the component and only 'successful' realisations are counted, i.e., realisations where the distances between the specified adjacent flaws are greater than the specified gaps $s_{i,i+1}$. For all such 'successful realisations' (Fig. 5), the specified minimum distances $s_{i,i+1}$ can be 'cut out' from the

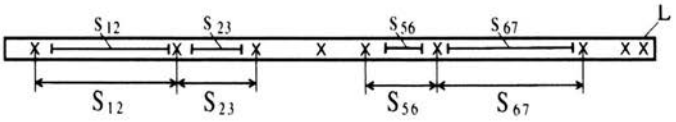

FIGURE 5.

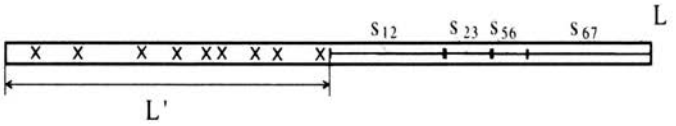

FIGURE 6.

actual flaw-free intervals $S_{i,i+1}$ between the selected k pairs of adjacent flaws and 'moved' towards the end of the component, as shown in Fig. 6.

Now, there exists a one-to-one correspondence between the *successful realisations*, in Fig. 5 (where the distances between the selected k pairs of adjacent flaws are at least s_{12}, s_{23}, s_{56}, and s_{67}) and the 'successful realisations' in Fig. 6 where 9 uniformly distributed flaws are generated over the entire length L and all fall over the shorter length $L' = L - \sum s_{i,i+1}$ ($L' = L - (s_{12} + s_{23} + s_{56} + s_{67})$, Fig. 6). Indeed, from all *successful realisations* of nine uniformly generated flaws over the length L (Fig. 5) with gaps greater than the specified minimum gaps between the selected adjacent flaws we can get all successful realisations of nine random flaw locations falling in the shorter length L'. This can be done by 'cutting out' the specified minimum distances $s_{i,i+1}$ between the corresponding adjacent pairs of defects and 'sticking' the cuts (Fig. 6). Conversely, from all *successful realisations* of nine uniformly generated flaws 'falling' only on the shorter length L' (Fig. 6), we can obtain all *successful realisations* in Fig. 5 (with the specified minimum distances $s_{i,i+1}$ between the selected pairs of flaws) simply by 'inserting' the specified minimum gaps $s_{i,i+1}$, between the corresponding adjacent flaws on the shorter length L'. In this way, the initial problem has been transformed into a simpler problem. Correspondingly, the probability of existence of the specified minimum gaps between the selected pairs of flaws is equal to the probability that from nine flaw locations generated uniformly over the length L, all locations will be within the shorter length L' only. Since the latter probability is given by Eq. (1.9) this is also the solution of our initial problem.

The distribution of the gap length x between any two adjacent flaws is given by

$$F(x) = 1 - (1 - x/L)^n, \tag{1.10}$$

which is a special case of Eq. (1.8). As can be verified easily, for a small ratio x/L or a large n, Eq. (1.10) transforms into the classical exponential distribution

$$F(x) = 1 - \exp[-(n/L)x] \tag{1.11}$$

which, in this case, is a very good approximation of the true distribution function (1.10). In the general case however, discrepancies exist between the results from Eq. (1.10) and (1.11) which are particularly large for large ratios x/L and a small number of flaws n.

Although, the case of a fixed number of random variables in a finite interval L has a number of useful practical applications (e.g. a fixed number of consumers connecting randomly during a day to a supply system which needs a minimum time interval s to recover [56]), of significant practical importance is the case where the number of flaws in the finite length L is a random variable (not known), [56].

1.4. Specifying the upper bound of the number density of Poisson-distributed flaws to guarantee probability of clustering below a maximum acceptable level

In most practical applications, the number of flaws in wire/fibre with finite length L is a random variable (unknown). If the distribution of flaws is a homogeneous Poisson process with intensity λ (flaw number density), the probability of a flaw-free length x is given by the classical formula (Montgomery et al., 2001)

$$p = \exp(-\lambda x). \tag{1.12}$$

The distribution of the gaps x between the flaws is given by the classical exponential distribution (Parzen, 1960): $F(x) = 1 - \exp(-\lambda x)$.

If the flaw locations follow a homogeneous Poisson process in the length L (the number of flaws in the finite length L is a random variable), Eq. (1.8) combined with the Poisson distribution can be used to derive the probability p_{MFFG} of a specified minimum flaw-free gap with length s between adjacent random flaws (Fig. 7).

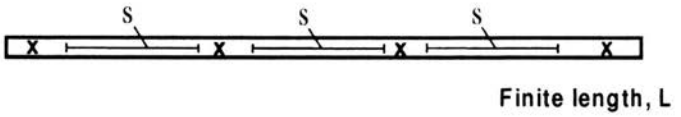

FIGURE 7.

Indeed, assume that the flaws follow a homogeneous Poisson process in the length L. The probability of k flaws in the finite length L is given by

the Poisson distribution $(\lambda L)^k \exp(-\lambda L)/k!$, $k = 0, 1, 2...$, where λL is the mean number of flaws in the finite length L (λ is the constant number density characterising the random flaws). According to the total probability theorem (Parzen, 1960), the probability that all adjacent flaws will be at distances greater than a specified minimum distance s apart from one-another is a sum of the probabilities of the mutually exclusive events 'k flaws are located in the finite length L and all of the adjacent flaws are at distances greater than the specified minimum distance s. The maximum number of flaw-free gaps of length s which can be accommodated in the finite length L is denoted by r ($r = [L/s] + 1$), where $[L/s]$ is the greatest integer which does not exceed the ratio L/s. The probability that between k adjacent flaws in the length L, there will be gaps greater than the specified minimum gap s is given by Eq. (1.8). Then, the probabilities that k random flaws will exist in the finite length L and between them there will be gaps greater than the specified minimum gap length s are: $\frac{(\lambda L)^k \exp(-\lambda L)}{k!} \times \left(1 - \frac{(k-1)s}{L}\right)^k$ for $1 \leq k \leq r$; $\exp(-\lambda L) \times 1$ for $k = 0$ and $\frac{(\lambda L)^k \exp(-\lambda L)}{k!} \times 0 = 0$, for $k > r$. The probability p_{MFFG} (probability of a minimum flaw-free gap) that wire with flaw density λ will not contain flaws clustering within a critical distance s (Fig. 7) then becomes, [56]

$$p_{MFFG} = \mathrm{e}^{-\lambda L}\left(1 + \lambda L + \frac{\lambda^2 (L-s)^2}{2!} + \ldots + \frac{\lambda^r [L-(r-1)s]^r}{r!}\right), \quad (1.13)$$

where $r = [L/s] + 1$. Correspondingly, the probability of clustering of two or more random flaws within a critical distance s is (Fig. 4):

$$p_c = 1 - \mathrm{e}^{-\lambda L}\left(1 + \lambda L + \frac{\lambda^2 (L-s)^2}{2!} + \ldots + \frac{\lambda^r [L-(r-1)s]^r}{r!}\right), \quad (1.14)$$

where $r = [L/s] + 1$.

By solving Eq. (1.14) numerically regarding λ (given a specified maximum acceptable probability of clustering $p_{c\max}$, the upper bound (the flaw density envelope) λ_c^* can be determined. The flaw number density envelope guarantees that whenever the flaw number density λ is within it ($\lambda \leq \lambda_c^*$) the specified minimum flaw-free gap s will exist with minimum probability $p_{MFFG} = 1 - p_{c\max}$ or, in other words, the probability of clustering will be smaller than the maximum acceptable value $p_{c\max}$.

In an illustrative example, the lineal density envelope will be determined which guarantees no clustering of flaws within a critical distance of 0.5 mm over a fibre of length 100 mm. The maximum acceptable probability of clustering has been specified to be $p_{c\max} = 0.1$. The upper bound of the flaw

number density is obtained by solving Eq. (1.13) with respect to the hazard rate λ where $p_{MFFG} = 1 - p_{c\max} = 0.9$. The obtained flaw density envelope is $\lambda_c^* = 0.0467$. Whenever the flaw number density λ is within the number density envelope ($\lambda \leq 0.0467$), the probability of clustering within a critical distance of 0.5 mm will be smaller than 0.1. Monte Carlo simulations (1000000 trials) of a homogeneous Poisson process with density $\lambda^* = 0.0467$ yielded 0.1 for the probability of clustering which illustrates the validity of Eqs. (1.13) and (1.14).

This result also means that for a mean number density 5 flaws in 100 mm length, the probability of clustering within a small distance of 0.5 mm is substantial (0.1). Even for the small mean number density of 2 flaws in 100 mm length, the calculations from Eq. (1.14) and the simulations show that there is still approximately 2% chance of clustering.

Figure 8 gives the dependence of the probability of clustering of flaws within a critical distance of $s = 1$ mm ($L = 100$ mm) for different values of the flaw number density. As can be verified from Fig. 8 for a flaw number density $\lambda = 0.014$ corresponding to 14 mean number of flaws per 100 mm length, the probability of clustering within a critical distance of 1mm is already 80%. This indicates that the probability of clustering increases quickly with increasing the flaw number density. These unexpected results demonstrate clearly that the probability of clustering of flaws following a homogeneous Poisson process in a finite interval is substantial and should always be taken

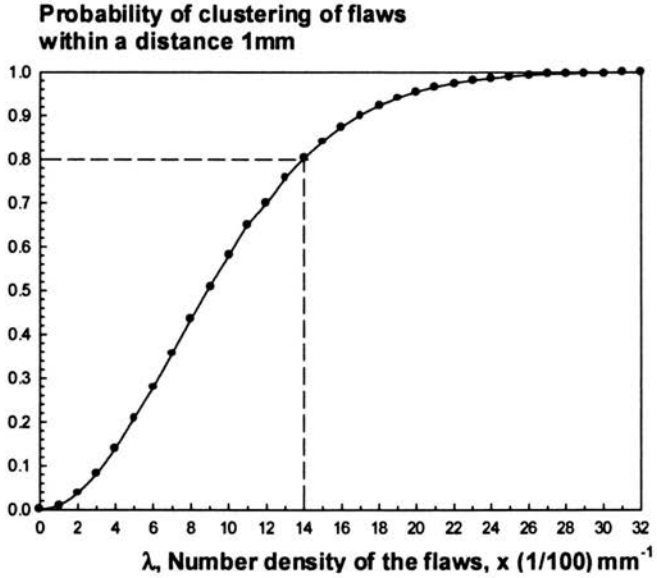

FIGURE 8.

into consideration in risk assessments. Solving Eq. (1.14) regarding the flaw number density, in fact specifies requirements regarding the maximum levels of material and manufacturing flaws which guarantee that the probability of failure due to clustering remains below a maximum acceptable level. The upper bound of the flaw number density (the flaw number density envelope) guarantees that whenever the actual flaw number density is within it, the probability of failure due to clustering remains below a maximum acceptable level.

2. Analysis of inhomogeneous microstructures using random transects

A powerful method of investigating inhomogeneous structures is by using random transects (point, linear and areal transects). These have been used in the quantitative microscopy for estimating a volume fraction and surface area of various microstructural constituents. Random transects for example, have been used in stereology for estimating the volume fraction of inhomogeneous microstructures (Weibel, 1980; Underwood, 1969). A line transect for example can be defined as a segment AB of given length L 'cast' in a random fashion (with an uniform distribution of the orientation angle γ and the coordinates of the mid point M) over a microstructural image (Fig. 9).

The ratio L_β/L of the length of the transect L_β lying in one of the microstructural constituents (e.g. β) to the entire length L of the transect is

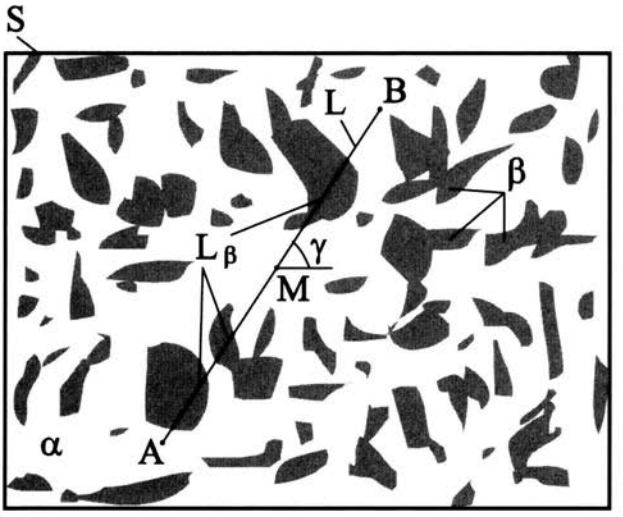

FIGURE 9.

referred to as *intercept*. For a three-dimensional transect, the intercept is defined as the ratio V_β/V_T of the volume V_β intercepted from one of the microstructural constituents (e.g. β) to the entire volume V_T of the transect. The distribution of the intercept is an important characteristic of duplex structures. For a duplex material containing two phases characterised by different density for example, the density distribution of a sample (transect) taken from the material will mirror the distribution of the intercept from the microstructural constituents.

The importance of the line transects for example can be illustrated by the Charpy V-notch test for determining the impact energy of steels. It has been demonstrated [67] that the type of microstructure in which the Charpy V-notch (line transect) is located during Charpy impact tests of multi-run C-Mn welds, has a crucial role on the distribution of the impact energy. If Charpy impact energy from inhomogeneous welds is examined, depending on the position of the notch on the sample, i.e. depending on which microstructural zone is sampled, distinct empirical cumulative distributions of the impact toughness are obtained, each characterising some of the existing microstructural zones. For structural integrity assessments, it is of particular interest to know the probability that the impact toughness will be within specified limits.

In many engineering structures, unexpected failures can often be attributed to the presence of crack-like defects located in microstructural regions characterised by low resistance to crack extension. Depending on the microstructural constituents or the local number density of the defects ahead of a crack front, the resistance to crack extension (the fracture toughness) varies widely.

2.1. Empirical cumulative distribution of the intercepts

The random variable X referred to as *intercepted fraction* or simply *intercept*, which accepts values $x = L_c/L$, where the index 'c' stands for one of the existing structural constituents (e.g. α or β) is an important tool for analysing inhomogeneous media. While the expected value $E(X)$ of the intercept X does not depend on the size of the transect (length, area, volume), its variance is a function of the transect size. The means of the intercepted fractions from one of the constituents (e.g. α), associated with transects of different size L are all unbiased estimates of the areal/volume fraction ξ_α of the α-constituent: $E(X) = \xi_\alpha$; $\xi_\alpha + \xi_\beta = 1$.

Indeed, let the transect with size L be divided into equal very small elements ΔL_j ($\Delta L_1 = \Delta L_2 = \ldots = \Delta L$), so small that it can be safely assumed that the probability of a particular ΔL_j sampling the α-constituent is

$P(\Delta L_j \in \alpha) \approx \xi_\alpha$ (the probability that ΔL will not sample α is $1-\xi_\alpha = \xi_\beta$). Consequently, each small element ΔL_j is associated with a random variable U_j indicating whether the element samples α-constituent or not. Therefore, the variables U_j have *Bernouli distribution* (DeGroot, 1989) defined as follows: U_j accepts '1' with probability ξ_α and '0' with probability ξ_β. Any line transect of arbitrary size L can be divided into q sufficiently small segments with lengths ΔL, where $q = L/\Delta L$. Then, for a random placement of the transect in the microstructure, the random variable 'intercepted fraction X' can be presented as

$$X = \frac{U_1\Delta L + U_2\Delta L + \ldots + U_q\Delta L}{q\Delta L} = \frac{1}{q}\sum_{j=1}^{q} U_j. \tag{2.1}$$

According to a well known result from the theory of probability (DeGroot, 1989), the expected value of a sum of random variables is equal to the sum of the expected values of the random variables irrespective of whether the variables are statistically independent or not (In fact U_j in Eq. (2.1) are correlated random variables since for any pair of adjacent small elements ΔL_j, and ΔL_{j+1}, if ΔL_j samples α, ΔL_{j+1} is also likely to sample α. Since the expected value of any U_j is $E(U_j) = 1 \times \xi_\alpha + 0 \times (1 - \xi_\alpha) = \xi_\alpha$, for the expected value $E(X)$ of the intercepted fraction, the expression

$$E(X) = \frac{1}{q}\sum_{j=1}^{q} E(U_j) = \frac{q\xi_\alpha}{q} = \xi_\alpha \tag{2.2}$$

is obtained. Consequently, the expected value of the intercepted fraction is equal to the areal/volume fraction of the α-constituent and does not depend on the length L of the transect.

The cumulative distribution function of the intercepted fraction $F(x, L)$ and the corresponding probability density function $f(x, L) = \partial F(x, L)/\partial x$ at a specified size L of the transect are important characteristics of inhomogeneous structures sampled by transects. Both functions depend on the size L of the transect.

Using the probability density function $f(x, L)$, Eq. (2.2) can be presented as

$$E(X) = \int_0^1 x f(x, L) dx = \xi_\alpha. \tag{2.3}$$

Only in trivial cases (e.g. for randomly distributed detached spheres β in matrix α) can the distribution functions $F(x, L)$ and $f(x, L)$ be obtained analytically (Kendall and Moran, 1963). In the general case (microstructural

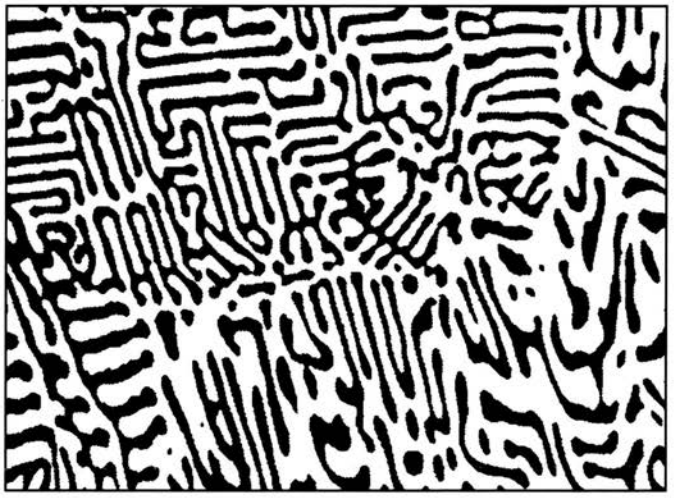

FIGURE 10.

constituents with irregular shape), the distributions can only be obtained by a Monte Carlo simulation involving sampling of images of the microstructure and registering the intercepted fractions.

Figure 10 is a scanned image of a cast microstructure (ASM, 1985). The lamellar eutectic contains dark zones (β-phase, $\xi_\beta = 0.4$) and white zones of (α-phase, $\xi_\alpha = 0.6$)

The image of the microstructure has been scanned as a bitmap file and read (Kay, 1995; Rimmer, 1993) by a computer simulation procedure. The longer side of the microstructural section used in the simulation, contains 640 length units. A random placement (random throw) of the transect was defined by three random numbers: two random coordinates of the middle point M and a random angle γ which the notch subtends with the horizontal axis (Fig. 9). The pixels along the line transect were scanned using the Bresenham algorithm (Hearn and Baker, 1997; Foley et al.,1996) and the number of pixels belonging to α, were counted. The intercept from α was calculated by dividing this number to the total number of pixels composing the transect. Empirical cumulative distributions of the intercepts from β, for different lengths of the line transect ($L = 80$, $L = 20$ and $L = 8$ units) are given in Fig. 11.

With increasing the size of the transect, the probability of intercepting almost entirely α or β decreases. With increasing the transect size, the probability of intercepting fractions far from the mean areal/volume fraction decreases, while the probability of intercepting fractions close to the mean areal/volume fraction increases. In other words, for large transects, the probability density function peaks at ξ_α and larger transects are associated with larger values of the probability density function at ξ_α.

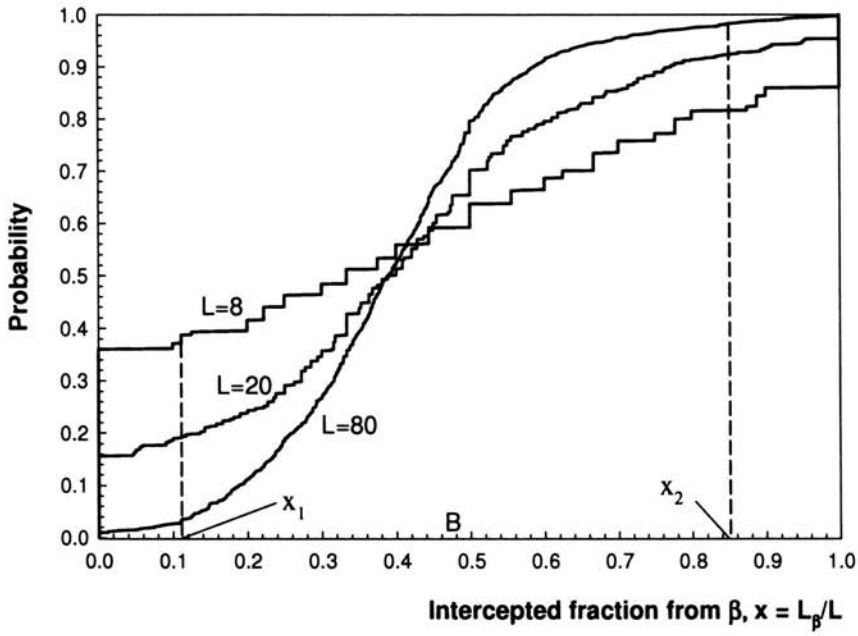

FIGURE 11.

Suppose for example, that intercepting a small amount x_1 by a transect compromises (causes a significant decrease) of the property value (e.g. the toughness of a specimen cut from a duplex material containing a though matrix and brittle particles which initiate cleavage fracture easily). The computer simulation results in Figure 11 show that although the probability that a small transect will sample a large amount of β is significant, small transects are associated with smaller probability of 'compromised toughness' because the probability $P(x \leqslant x_1)$ is larger (Fig. 11). Next, suppose that the property value is compromised substantially only if the line transect intercepts a relatively large amount x_2 (Figure 11). This is for example the case where the yield strength of a specimen cut from duplex material containing hard and soft constituents is compromised if too much soft constituent β has been sampled.

Then, as can be seen from Figure 11, small size transects are associated with a higher probability of intercepting large fractions of β and compromised yield strength.

Since the distribution of properties is significantly influenced by the distribution of intercepts, the empirical cumulative distribution of the intercepts is an important fingerprint of inhomogeneous structures and contains valuable information regarding the risk of poor properties.

2.2. Intercept variance

The variance of the intercepted fraction denoted by $V_c(X, L)$, $(c \in \{\alpha, \beta\})$ is another important characteristic of inhomogeneous media. The variance is a function of the size of the transect and for a transect of particular size L, it is defined by the integral:

$$V_c(X, L) = \int_0^1 f(x, L)[x - \xi_c]^2 dx = \int_0^1 x^2 f(x, L)dx - \xi_c^2, \qquad (2.4)$$

obtained using the well-known formula (DeGroot, 1989) for a variance of a random variable X with mean μ, $V(X) = E(X - \mu)^2 = E(X^2) - \mu^2$. The integral in the right hand side of Eq. (2.4) is the expected value of the squared intercept ($\int_0^1 x^2 f(x, L)dx = E(X^2)$). For a transect of zero size ($L = 0$) which consists of a single point, the probability density distribution $f(x, 0)$ of the intercept X is the discrete *Bernouli distribution* with parameter ξ_α, i.e., the intercepted fraction is '1' with probability ξ_α and '0', with probability $1 - \xi_\alpha$. The variance of the intercepted fraction X from α becomes

$$V_\alpha(X) = E(X^2) - [E(X)]^2 = \xi_\alpha - \xi_\alpha^2 = \xi_\alpha \xi_\beta, \qquad (2.5)$$

because $E(X) = 1 \times \xi_\alpha + 0 \times \xi_\beta = \xi_\alpha$ and $E(X^2) = 1^2 \times \xi_\alpha + 0^2 \times \xi_\beta = \xi_\alpha$.

For an infinitely large transect L and random microstructure without anisotropy, the transect intercepts a constant fraction $x = \xi_c$ and the variance $V_c(X, L)$ from Eq. (2.4) becomes zero. The relationship between the

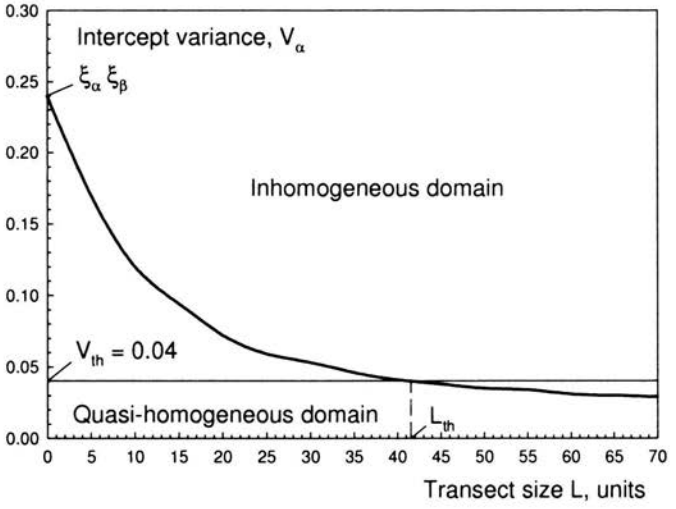

FIGURE 12.

variance of the intercepted fraction and the size L of the transect (Fig. 12), is an important fingerprint of inhomogeneous microstructures. If for example, a variance of the intercept smaller than a particular threshold (e.g. $V_{th} = 0.04$ in Fig. 12) causes negligible variation in the property value, the material behaves like quasi-homogeneous. Whether the material will behave like a quasi-homogeneous or inhomogeneous depends on the size of the transect. The intersection of the horizontal line corresponding to the variance threshold V_{th} with the graph of the intercept variance determines a limiting transect size L_{th} (Fig. 12). Accordingly, the same microstructure sampled with transects larger or smaller than L_{th} can exhibit a 'quasi-homogeneous' or 'inhomogeneous' behaviour. Thus, the variances of the intercepts characterising the different transect lengths ($L = 80$, $L = 20$ and $L = 8$) in Fig. 11 are 0.029, 0.073 and 0.144, respectively. They were calculated from $V = \frac{1}{N}\sum_{i=1}^{N}(x_i - \xi_\beta)^2$, where N is the number of trials (6000 in the simulation); x_i is the intercept from β at the i-th random placement of the transect; $\xi_\beta = 0.4$ is the areal/volume fraction of the β-constituent which is also the mean of the intercepts x_i.

An important characteristic of the intercept variance is the average slope $\Delta V/\Delta L$ (Fig. 12) which measures the change of the intercept variance per unit increment of the transect size. The slope is negative since the intercept variance decreases monotonically with increasing the size of the transect. If the absolute value of the slope of the intercept variance is large (the intercept variance decreases quickly with increasing the transect size), relatively small transect sizes are sufficient to 'stabilise' the intercept variance at a low level, which guarantees consistent intercept and property values. Such type of intercept variance function is typical for fine-grained duplex structures (Fig. 13).

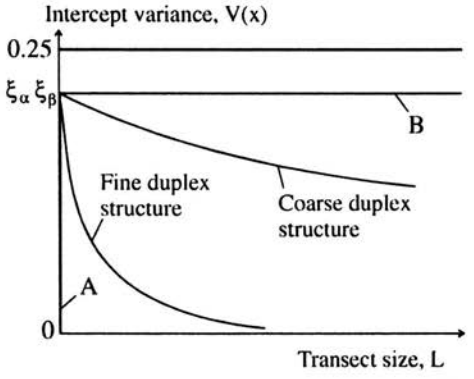

FIGURE 13.

Conversely, if the intercept variance decreases slowly with increasing the size of the transect, large transects are necessary to stabilise the intercept variance at a low level and obtain consistent intercept and property values. Such type of intercept variance function for example, is typical for coarse-grained duplex structures.

As a result, the graph of the intercept variance has an important application: calculating the minimum size of the sampler that stabilises the variation of the intercept (and the property correlated with the intercept) at low values. The intercept variance from sampling any inhomogeneous microstructure varies between the intercept variance of an ideal fine dispersed structure (Fig. 13, the vertical line A) and an ideal coarse-grained structure (Fig. 13, the horizontal line B). The intercept variances of the fine-grained structures are shifted towards the vertical line A, where very small transect sizes can stabilise the variance (and the correlated property) at a low level. Conversely, intercept variances characterising coarse-grained structures are shifted towards the horizontal line B, where relatively large transect sizes are needed to stabilise the variance (and the associated property) at a low value.

The intercept variance depends on the size of the transect and decreases monotonically from $\xi_\alpha\xi_\beta$ to 0, since larger transects are characterised by a smaller variance of the intercepted fraction. The intercept variance cannot exceed the value $\xi_\alpha\xi_\beta = \xi_\alpha(1-\xi_\alpha)$ and since the maximum of $\xi_\alpha(1-\xi_\alpha)$ is attained for $\xi_\alpha = 0.5$, for any type of duplex structure, the intercept variance cannot exceed the absolute upper bound $V_{\max} = 0.25$. This is obtained for the smallest transects, with zero size, sampling duplex microstructures for which $\xi_\alpha \approx 0.5$.

Although all transect sizes produce unbiased estimates of the volume fraction of the microstructural constituents, the estimates from large transects are characterised by small errors. The scatter of properties depends significantly on the size of the transect. The common classification of a microstructure into 'quasi-homogeneous' or 'inhomogeneous' is conditional. Depending on the size of the transect and on the way of sampling, a 'fine-grained' microstructure can be characterised by a scatter typical for a coarse-grained microstructure. Conversely, a coarse inhomogeneous microstructure can be characterised by a very small scatter of the properties, typical for a fine-grained inhomogeneous microstructure.

An important application of the concept 'intercept variance' is the topological optimisation of a microstructure where for a specified probability distribution $p(x)$ of the transect size, the distribution and the shape of the second microstructural constituent is varied until the intercept variance in Eq. (2.4) is minimised. In another example of a topological optimisation, a particular distribution of the second microstructural constituent may be

sought which minimises the probability that a random transect of a specified size will sample more than a certain fraction from the weaker constituent.

The empirical cumulative distribution of the intercepts and their variance are important fingerprints of inhomogeneous media [59]. They constitute the basis of new methods for structural integrity assessment and can be used for quantifying levels of acceptable risk which is one of the major challenges to the reliability engineering today.

3. Analysis of inhomogeneous microstructures formed by nucleation and growth using random transects

Transects of different shapes and sizes can be applied to analyse inhomogeneous microstructures formed by nucleation and growth. The nuclei crystallised from one of the constituents do not cover the entire system (partially crystallised materials or materials where the rate of crystallisation is so slow that they are in fact duplex materials).

A typical feature of these microstructures is that they are formed by nuclei (β) arising and growing in a matrix (α). The nucleation and growth are contained in a system with finite volume V.

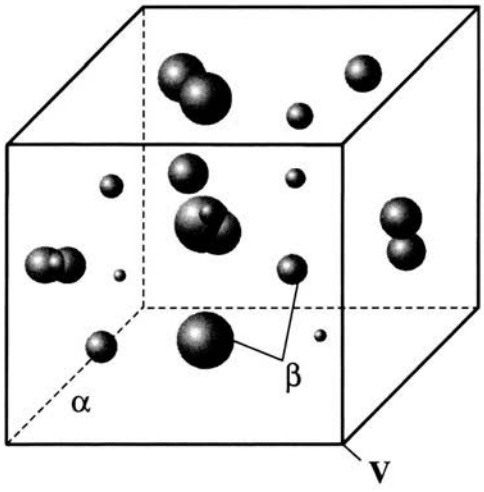

FIGURE 14.

It is assumed that the growth rate is isotropic (the growth rate is the same in any direction). The growth stops at the points of contact of the growing nuclei (growth with impingement). Topologically, the duplex structure in the finite volume V can be composed of interpenetrating spherical nuclei β, uniformly distributed in the finite volume V. The nuclei arise with a time-

dependent rate $I(\tau)$ in the α-phase and grow with a constant radial rate k. The number dN of newly formed nuclei in the time interval $(\tau, \tau + d\tau)$ is proportional to the volume of the remaining α-phase: $dN = I(\tau)V_\alpha d\tau$.

There exists equivalence between the kinetics of a phase transformation of the type 'nucleation and growth with a constant radial rate and the process of continuous coverage of space by overlapping spheres growing with a constant radial rate, [69]. This allows us, instead of simulating the nucleation in α-phase whose volume fraction changes constantly, to simulate the nucleation in the system volume V which is constant. Those nuclei, which 'arise' in already transformed phase are 'imaginary' and do not contribute to the quantity of transformed phase since, due to the constant growth rate their boundary can never cross the boundary of the nucleus into which they 'nucleated'. Because of this formalism, the number of real nuclei (those which nucleate in α) at any time is proportional to the volume of the remaining α-phase. As a result, nucleation and growth with a constant radial rate is mathematically equivalent to a coverage of space by overlapping spheres growing with a constant radial rate. The number of spherical nuclei appearing in the infinitesimal interval $\tau, \tau + d\tau$ is given by $dN = I(\tau)V d\tau$.

3.1. Analysis of an inhomogeneous microstructure formed by nucleation and growth by a random transect of zero length

The probability that a random transect of zero length (a randomly selected point) will sample α-phase only is equal to the probability that none of the nuclei that have appeared in the time interval $(0, \tau)$ cover the selected point.

Suppose, that the time at which the microstructure is being analysed is τ. The probability that none of the nuclei with radii $k\nu$ that have appeared in

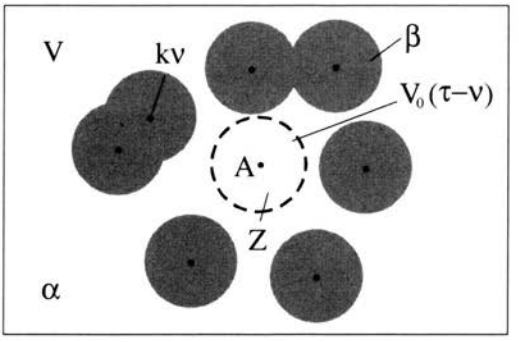

FIGURE 15.

the infinitesimal time interval $(\tau-\nu, \tau-\nu+d\nu)$ cover the transect (point A) is given by

$$[1-(4/3)\pi k^3\nu^3/V]^{VI_{t-\nu}d\nu} = \exp\{VI_{\tau-\nu}d\nu \ln[1-(4/3)\pi k^3\nu^3/V]\}, \quad (3.1)$$

$(\exp\{SI_{\tau-\nu}d\nu \ln[1-\pi k^2\nu^2/S]\}$ in the two-dimensional case; S is the area of the system), where $I_{\tau-\nu}$ is the nucleation rate at the instant $\tau-\nu$ and $k\nu$ are the radii of the nuclei that have appeared at time $\tau-\nu$ (ν is a time increment). This is essentially the probability that all nuclei which have appeared in the time interval $(\tau-\nu, \tau-\nu+d\nu)$ will lie outside the exclusion volume $V_0(\tau-\nu)$ (Fig. 15), in the volume $V-V_0$. The probability that none of the nuclei that have appeared in the time interval $(0,\tau)$ cover the transect A is a product of the probabilities of 'non-coverage' characterising all portions of nuclei that have appeared in the time interval $(0,\tau)$. Hence, the probability ξ_a that the transect A will sample α-phase only is

$$\xi_a = \exp\left(\int_0^\tau VI_{t-\nu}\ln[1-(4/3)\pi k^3\nu^3/V]d\nu\right) \quad (3.2)$$

in the three-dimensional case, where V is the finite volume of the system (ν is a dummy integration variable). In the two-dimensional case, the equation corresponding to Eq. (3.2) is $\xi_a = \exp\left(\int_0^\tau SI_{\tau-\nu}\ln[1-\pi k^2\nu^2/S]d\nu\right)$, where S is the area of the finite system where the nucleation takes place. Since $\xi_a+\xi_\beta = 1$, the quantity of the transformed phase is given by [69]

$$\xi_\beta(\tau) = 1-\exp\left(\int_0^\tau VI_{\tau-\nu}\ln[1-(4/3)\pi k^3\nu^3/V]d\nu\right). \quad (3.3)$$

For a system of finite unit volume ($V=1$) Eq. (3.3) transforms into

$$\xi_\beta(\tau) = 1-\exp\left(\int_0^\tau I_{\tau-\nu}\ln[1-(4/3)\pi k^3\nu^3]d\nu\right), \quad (3.4)$$

and describes kinetics of phase transformation with a constant radial growth rate in a system of finite volume. If the nucleation rate is constant ($I_\tau \equiv I = \text{const}$), Eq. (3.4) transforms into

$$\xi_\beta(\tau) = 1-\exp\left(I\int_0^\tau \ln[1-(4/3)\pi k^3\nu^3]d\nu\right). \quad (3.5)$$

Often, the quantity of transformed phase (under the same conditions under which Eq. (3.5) has been derived) is given by the Kolmogorov–Johnson–Mehl–Avrami equation (Kolmogorov, 1937; Johnson and Mehl, 1939; Avrami, 1939, 1940, 1941) (KJMA equation):

$$\xi_\beta(\tau) = 1 - \exp[-(\pi/3)Ik^3\tau^4], \tag{3.6}$$

where I is a constant nucleation rate and k is a constant radial growth rate.

3.2. Limitations of the Kolmogorov–Johnson–Mehl–Avrami equation

It must be pointed out that for a phase transformation in a finite volume, the JMAK equation (3.6) is not exact, and for a small number of growing nuclei in the system, the quantity of the transformed phase calculated from it shows significant deviations from the Monte Carlo simulations [65]. The smaller the number of growing nuclei is, the greater is the deviation of the transformed fraction predicted by the JMAK equation (3.6) from the true transformed fraction given by Eq. (3.5). This can be verified immediately from the JMAK equation (3.6) which describes a process which requires infinite time τ for completion, while the corresponding geometrical process of transformation (coverage) is, in fact, finite.

Indeed, assume that the system where the phase transformation takes place, is a sphere of unit volume ($V = 1$). Suppose that a spherical nucleus arises at time $\tau = 0$ in the centre of the sphere. It is clear, that after the instant $\tau^* = (1/k)\sqrt[3]{3/(4\pi)}$, no untransformed (uncovered) parts of the system will exist, i.e. $\xi_\beta(\tau^*) = 1$ because at time τ^* the radius of the growing nucleus will become equal to the radius of the system. Substituting τ^* in Eq. (3.6) however, results in a quantity less than unity: $\xi_\beta(\tau^*) = 1 - \exp[-I\sqrt[3]{3/(4\pi)}/(4k)] < 1$, which contradicts to the above simple geometrical consideration. This contradiction is due to the restricted applicability of the JMAK equation. It gives a good approximation only in cases where the number of growing nuclei in the system is large or for the stages of the transformation where the ratios of the volumes of the growing nuclei to the volume of the system are small. If the volume ratios of the growing nuclei are small, the JMAK equation approximates very well the true transformed fraction and is a special case of the exact equation (3.5). This is indeed the case at the beginning of the transformation and when the system contains a very large number of nuclei so that the transformation is completed before the nuclei can reach large volume ratios. Indeed, for a small volume fraction $(4/3)\pi k^3\nu^3/V$, $\ln[1 - (4/3)\pi k^3\nu^3] \approx -(4/3)\pi k^3\nu^3$

and Eq. (3.5) transforms into the JMAK equation (3.6). If the system contains a small number of nuclei with relatively large volume ratios however, no matter how large the volume of the system is, the predictions from the JMAK equation deviate from the true transformed fraction given by Eq. (3.5). In this case, the exact equation (3.5) should be applied instead of the JMAK equation (3.6). Equation (3.5) is particularly useful for calculating transformed fraction from growth of very small number of nuclei in a finite volume V.

3.3. Illustrative examples

For the simplified example where n nuclei start their growth at time $\tau = 0$, and no other nuclei arise subsequently, the transformed fraction $\xi_\beta(\tau)$ at any time τ is equal to the probability $\xi_\beta(\tau)$ that for any fixed point A, at least a single nucleus has nucleated inside a sphere of radius $k\tau$. This probability is given by:

$$\xi_\beta(\tau) = 1 - \left(\frac{V - (4/3)\pi k^3\tau^3}{V}\right)^n = 1 - \exp\left\{n \ln\left[1 - \frac{(4/3)\pi k^3\tau^3}{V}\right]\right\}$$

which can also be presented as

$$\xi_\beta(\tau) = 1 - \exp(n \ln[1 - \psi(\tau)]), \tag{3.7}$$

where $\psi(\tau) = (4/3)\pi k^3\tau^3/V$. Equation (3.7) is an analogue of Eq. (3.5). It also describes the covered fraction by n overlapping objects of equal volume ratios $\psi(\tau)$. (For a random coverage with overlapping objects, the covered volume fraction $\xi(\tau)$ in Eq. (3.7) depends only on the volume ratio $\psi(\tau)$ and does not depend on the shape of the objects). In case of a small volume ratio $\psi(\tau)$, the approximation

$$\ln[1 - \psi(\tau)] \approx -\psi(\tau) \tag{3.8}$$

is possible and Eq. (3.7) transforms into

$$\xi_\beta(\tau) = 1 - \exp[-n\psi(\tau)] \tag{3.9}$$

which is a version of the JMAK equations (3.5). If the number of nuclei n in the controlled volume V is large, the transformation terminates (ξ_β approaches unity) at relatively small nuclei volumes $(4/3)\pi k^3\tau^3$. As a result, the volume ratio $\psi(\tau) = (4/3)\pi k^3\tau^3/V$ remains small during the transformation and approximation (3.9) is possible. However, if the number of nuclei in V is small, after the initial stage of the transformation, the volume ratio of the nuclei $\psi(\tau) = (4/3)\pi k^3\tau^3/V$ is no longer small. Due to the sparse nuclei,

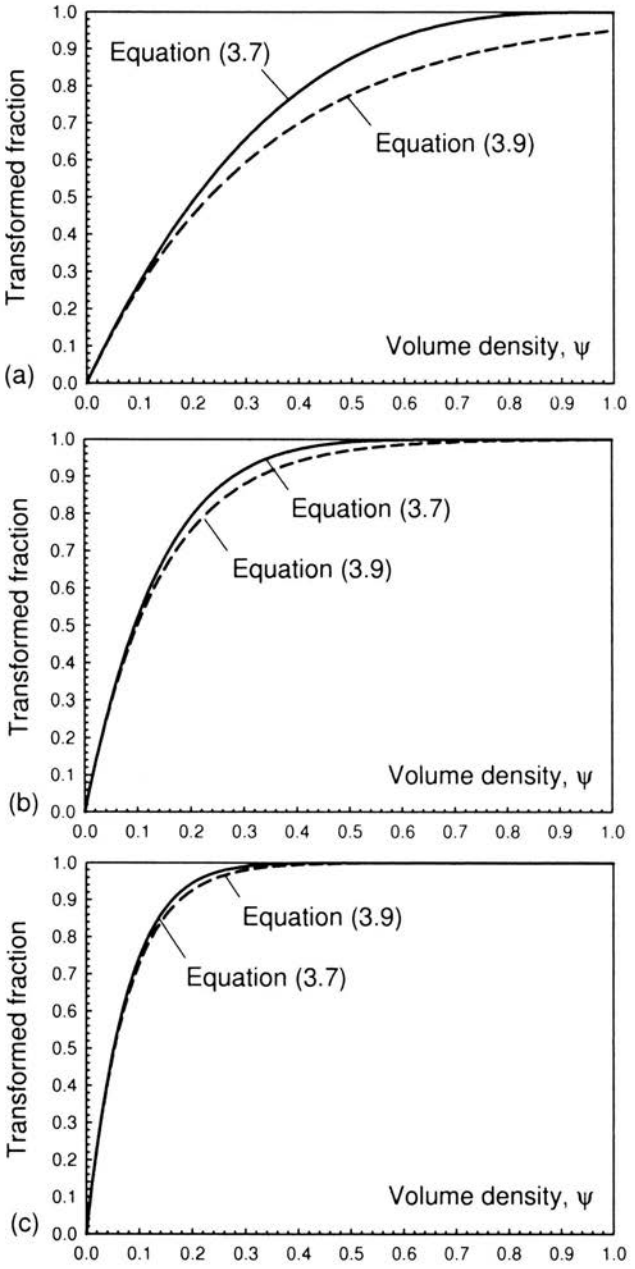

FIGURE 16.

at some instant τ the volume $(4/3)\pi k^3\tau^3$ of the growing nuclei will become comparable with V. Consequently, approximation (3.8) is no longer possible and Eq. (3.7) instead of Eq. (3.9) should be applied.

The difference between Eqs. (3.7) and (3.9) (also between Eqs. (3.5) and (3.6)) becomes apparent if their graphs are compared for $n = 3$ (Fig. 16(a)), $n = 7$ (Fig. 16(b)), and $n = 13$ (Fig. 16(c)). In all three graphs, the volume fraction is plotted versus the volume ratio ψ of the nuclei. As can be verified, the difference between the graphs of Eq. (3.7) and Eq. (3.9) diminishes substantially for small volume ratios and also for a large number of nuclei. Indeed, the difference between the right hand parts of Eqs. (3.7) and (3.9) is $\Delta = \exp[n\ln(1-\psi(\tau)] - \exp[-n\psi(\tau)]$ and for small $\psi(\tau)$, $\exp[n\ln(1-\psi(\tau)] \approx \exp[-n\psi(\tau)]$ and $\Delta \approx 0$. For large n, both terms in the difference are very small ($\exp[n\ln(1-\psi(\tau)] \approx 0$ and $\exp[-n\psi(\tau)] \approx 0$) and again $\Delta \approx 0$. For a small number of nuclei, (e.g. $n = 3$) the differences are substantial.

It must be pointed out, that the discrepancies in the predictions from the JMAK equation depend on the number of growing nuclei and do not depend directly on the nucleation and growth rate. Thus, at fixed nucleation and growth rates, if the controlled volume is such that it contains a small number of growing nuclei, discrepancies will exist. If the controlled volume is being increased progressively so that it contains more growing nuclei, better agreement will be obtained between the predictions from the JMAK equation and the true transformed fraction. Beyond a certain number of nuclei in the controlled volume, the agreement will be almost perfect.

3.4. Probability of sampling matrix phase only by a line transect of finite length

Similar to the derivation in Sec. 3.1, the probability that a randomly cast linear segment (line transect) with length x will sample only α-phase is equal to the probability that none of the nuclei that have appeared in the time interval $(0,\tau)$ intersects the line transect.

The probability that none of the nuclei with radii $k\nu$ that have appeared in the infinitesimal time interval $(\tau-\nu, \tau-\nu+d\nu)$ intersects the line transect is given by

$$\{1 - [\pi k^2\nu^2 x + (4/3)\pi k^3\nu^3]/V)\}^{V I_{t-\nu} d\nu} = \exp\{V I_{\tau-\nu} d\nu \ln[1 - (\pi k^2\nu^2 x + (4/3)\pi k^3\nu^3)/V]\},$$

($\exp\{S\, I_{\tau-\nu} d\nu \ln[1-(\pi k^2\nu^2+2k\nu x)/S]\}$ in the two-dimensional case), where $I_{\tau-\nu}$ is the nucleation rate at the instant $\tau-\nu$ and $k\nu$ is the radius of the

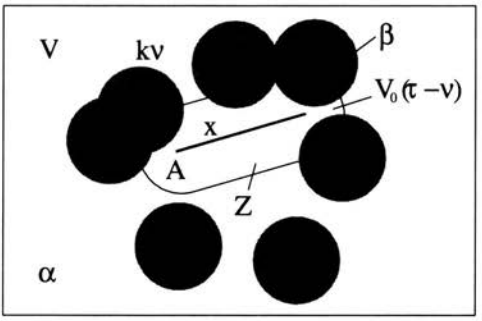

FIGURE 17.

nuclei that have nucleated at time $\tau - \nu$ (ν is a time increment). This is again the probability that all nuclei which have appeared in the time interval $(\tau - \nu, \tau - \nu + d\nu)$ will lie outside the exclusion volume $V_0(\tau - \nu)$ (Fig. 17), in the volume $V - V_0$. The probability that none of the nuclei that have appeared in the time interval $(0,\tau)$ intersects the line transect is a product of the probabilities of 'non-intersection' characterising all portions of nuclei that have appeared in the time interval $(0, \tau)$. Assuming a unit volume $V = 1$, the probability $T(x)$ that the line transect with length x will sample α-phase only is [53]:

$$T(x) = \exp\left(\int_0^{\tau} I_{t-\nu} \ln[1 - ((4/3)\pi k^3 \nu^3) + \pi k^2 \nu^2 x)] d\nu\right) \tag{3.10}$$

in the three-dimensional case, where V is the finite volume of the system (ν is a dummy integration variable). In the two-dimensional case, the equation corresponding to Eq. (3.10) is $T(x) = \exp\left(\int_0^{\tau} I_{\tau-\nu} \ln[1 - (\pi k^2 \nu^2 + 2kx\nu)] d\nu\right)$ where the finite area of the system where the nucleation takes place has been taken to be unity. The probability that the transect with length x will be intersected by at least a single nucleus is $1 - T(x)$. For a transect with zero length $x = 0$ (a single-point transect), the expression for $T(x)$ gives the volume fraction ξ_a of the α-phase. and Eq. (3.10) transforms into Eq. (3.4).

3.5. Probability of sampling matrix phase only by a transect (2D, 3D) of arbitrary shape

The equation giving the probability that a random transect (2D or 3D) of arbitrary shape will intercept matrix phase only is given by

$$T(x) = \exp\left(\int_0^{\tau} I_{t-\nu} \ln[1 - \psi(\nu)] d\nu\right), \tag{3.11}$$

where $\psi(\nu)$ is the volume fraction of the exclusion zone $V_0(\tau - \nu)$ for nuclei which appeared in the infinitesimal time interval $(\tau - \nu, \tau - \nu + d\nu)$, Fig. 18.

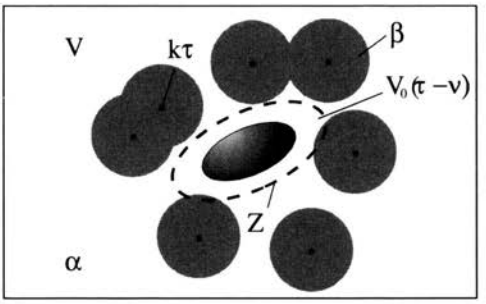

FIGURE 18.

The derivation is similar to the derivation of Eq. (3.10). The probability that none of the nuclei with radii $k\nu$ that have appeared in the infinitesimal time interval $(\tau - \nu, \tau - \nu + d\nu)$ will intersect the 3D-transect is

$$\{1 - V_0(\tau)/V\}^{V I_{t-\nu} d\nu} = \exp\{V I_{\tau-\nu} d\nu \ln[1 - V_0(\tau - \nu)/V]\},$$

where $I_{\tau-\nu}$ is the nucleation rate at the instant $\tau - \nu$ and $V_0(\tau - \nu)$ is the volume of the exclusion zone for nuclei that have nucleated at time $\tau - \nu$ (ν is a time increment). This is essentially the probability that all nuclei which have appeared in the time interval $(\tau - \nu, \tau - \nu + d\nu)$ will lie outside the exclusion volume $V_0(\tau - \nu)$ (Fig. 18), in the volume $V - V_0$. The probability that none of the nuclei that have appeared in the time interval $(0, \tau)$ will intersect the transect is a product of the probabilities of 'non-intersection' characterising all portions of nuclei that have arisen in the time interval $(0, \tau)$. Denoting $\psi(\nu) = V_0(\tau - \nu)/V$ and assuming a unit volume $V = 1$, the probability $T(x)$ that the line transect will sample α-phase only is given by Eq. (3.11).

3.6. Probability of a minimum free path in the matrix

For arbitrary two-phase microstructure formed by nuclei following a homogeneous Poisson process, there exists a link between the probability $P(x) = 1 - F(x)$ that the free path from a point in the matrix will be

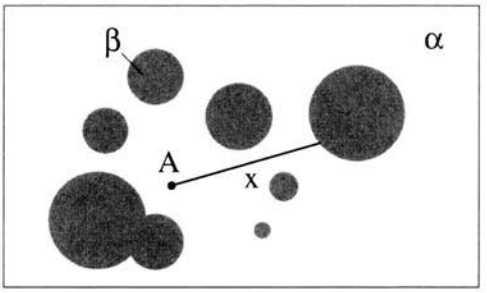

FIGURE 19.

greater or equal than a specified length x and the probability $T(x)$ of sampling matrix phase only by a line transect of length x. The link between the two probabilities can be found using the following probabilistic argument.

The probability $T(x)$ is a product of the probabilities of two events. The first event: 'a particular selected end of the transect (e.g. the end A in Fig. 19) samples α' is characterised by probability ξ_α which is the volume fraction of the α phase. The probability of the second event 'the continuation of the transect will be longer than x given that the end A samples α phase' is in fact the probability $P(x)$ of existence of a free path of minimum length x.

As a result we get

$$T(x) = \xi_\alpha P(x). \tag{3.12}$$

Considering that $P(0) = 1$, From Eq. (3.12) it follows that $T(x = 0) = \xi_a \times P(x = 0)$, from Eq. (3.12) it follows that $T(0) = \xi_a$. Equation (3.12) can also be presented as:

$$P(x) = \frac{T(x)}{T(0)} \tag{3.13}$$

which provides a link between three fundamental characteristics of inhomogeneity [53].

Indeed, consider a case where the second phase β is formed by a large number of overlapping equal-sized circular nuclei with radii R in a plane (Fig. 20).

The probability $P(x)$ that a path starting in α, will be longer than x (Fig. 20) is

$$P(x) = 1 - F(x) \approx \exp(-2\lambda x R), \tag{3.14}$$

where λ is the areal number density of the nuclei. This is in fact the probability that the centres of all nuclei will lie outside the exclusion zone Z with area $2Rx$ (Fig. 20). Similarly, the probability $T(x)$ that a transect of size x will sample α only is given by $T(x) \approx \exp[-\lambda(2xR + \pi R^2)]$. The latter

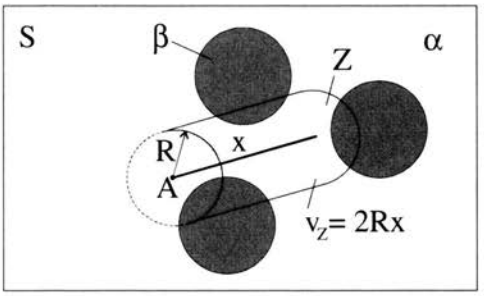

FIGURE 20.

expression can also be rearranged as $T(x) = \exp(-2\lambda x R)\exp(-\lambda\pi R^2) = \xi_\alpha \exp(-2\lambda x R) = \xi_\alpha P(x)$ [53], which is exactly Eq. (3.12). From Eq. (3.14), it follows that microstructures characterised by the same value of the product (*number density of the nuclei* $\times$ *nuclei projection size on a plane perpendicular to the free path*, $\lambda \times 2R$) are characterised by the same probability $P(x)$ that the free path in the matrix will be greater than x. It can be also shown that a similar statement is also valid for the three-dimensional case. Indeed in the three dimensional case $T(x) \approx \exp[-\lambda(\pi R^2 x + (4/3)\pi R^3)]$. Because $\xi_a = \exp[-\lambda(4/3)\pi R^3]$, the expression regarding the transect can be presented as

$$T(x) = \xi_\alpha \exp(-\lambda\pi R^2 x) = \xi_\alpha P(x). \tag{3.15}$$

As can be verified from Eq. (3.15), microstructures characterised by the same value of the product (*number density of the nuclei* $\times$ *nuclei projection area on a plane perpendicular to the free path*, $\lambda \times \pi R^2$) are characterised by the same probability $P(x)$ that the free path in the matrix will be greater than x [53].

It can be shown also that for arbitrary nuclei sizes, increasing the number density of the nuclei and decreasing the size of the mean projection of the nuclei (on a plane perpendicular to the free path) by the same factor does not affect the mean and the variance of the free paths in the matrix phase [53]. For an arbitrary convex shape of the nuclei it has been shown in [53] that the probability that a transect of size x will lie in α phase is given by

$$T(x) = \exp[-\lambda(\bar{t}x + s)], \tag{3.16}$$

where $\bar{t}$ is the mean calliper diameter of a single 2D-nucleus or the mean projection area of a single 3D-nucleus on a plane perpendicular to the direction of the transect in the 3D-case. In Eq. (3.16), λ is the number density of the nuclei and s is the area of a single nuclei.

4. Statistics of properties of inhomogeneous materials

4.1. The importance of the shape of the lower tail of material property distributions

A common framework for predicting structural/mechanical reliability at a component level is the load-strength (demand-capacity) interference (Freudenthal, 1954; Carter, 1986) which deals with the interaction of the load distribution with the strength distribution.

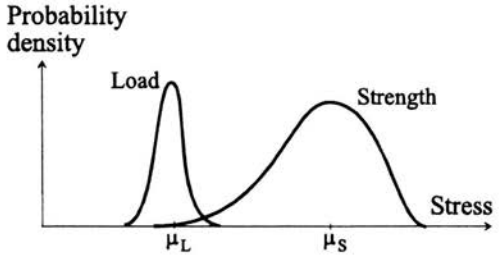

FIGURE 21.

Numerous failure modes can be described conveniently in the context of the load-strength interference (Freudenthal, 1954; Carter, 1986). Such are for example all cases where failure occurs whenever the load exceeds resistance. The reliability in this case is determined by the probability that the load L will be smaller than the strength S ($P(L < S)$). The strength variation is a complex function of *material properties*, *design configuration* and *geometry*. A long and thick lower tail in the material property distribution usually yields a long and thick lower tail of the strength distribution which entails low reliability. Low values of the material property exert stronger influence on reliability than do high or intermediate values.

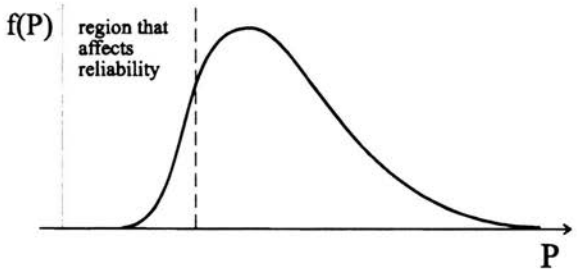

FIGURE 22.

An adequate model of the material properties should faithfully represent the lower tail of the corresponding distribution.

An important reliability parameter for load and strength following the normal (*Gaussian*) distribution is the *safety margin* β defined by

$$\beta = \frac{\mu_S - \mu_L}{\sqrt{\sigma_S^2 + \sigma_L^2}}, \tag{4.1}$$

where μ_S and μ_L are the mean strength and the mean load and σ_S and σ_L are the standard deviations of the strength and the load, correspondingly. Reliability (the probability that the load will be smaller than the strength) is determined from (Christensen and Baker, 1982)

$$R = 1 - \Phi(-\beta), \tag{4.2}$$

where $\Phi(\bullet)$ denotes the cumulative distribution function of the standard normal distribution. The safety margin is a measure of the relative separation of the load and strength is an important reliability parameter for normally distributed load and strength and. The larger the difference $\mu_S - \mu_L$ and the smaller the standard deviations of the strength and the load, the larger is the reliability R. It must be pointed out however, that the safety margin is valid *only for normally distributed load and strength.* The normal distribution however rarely describes satisfactorily the material property variation in the distribution tails. Some of the more obvious reasons are:

- the distribution of materials properties is usually asymmetric, skewed to the right while the normal distribution is symmetric,
- the normal distribution is unbounded on the left, while the material property distribution *is always bounded on the left.* A probabilistic design analysis based on a normal model for the material property P can be inaccurate. The *Weibull model* and the *Log-normal model* are often suitable models for the variation of materials properties but often the material property distribution is in effect a distribution mixture.

For non-normally distributed load and strength, the safety margin is misleading. Figure 23 illustrates a case where a low safety margin $\beta = \frac{\mu_S - \mu_L}{\sqrt{\sigma_S^2 + \sigma_L^2}}$ exists ($\mu_S - \mu_L$ is small and $\sigma_S^2 + \sigma_L^2$ is large) yet the reliability is high.

The next figure (Fig. 24) is obtained by reflecting symmetrically the distributions in Fig. 23. Since a mirror reflection does not change the variances of the distributions, the only difference is the larger difference of the means $\mu'_S - \mu'_L > \mu_S - \mu_L$. As a result, a new, larger safety margin β' is obtained: $\beta' = \frac{\mu'_S - \mu'_L}{\sqrt{\sigma_S^2 + \sigma_L^2}} > \beta = \frac{\mu_S - \mu_L}{\sqrt{\sigma_S^2 + \sigma_L^2}}$ despite the fact that the reliability associated with the distributions in Fig. 24 is smaller than the reliability associated

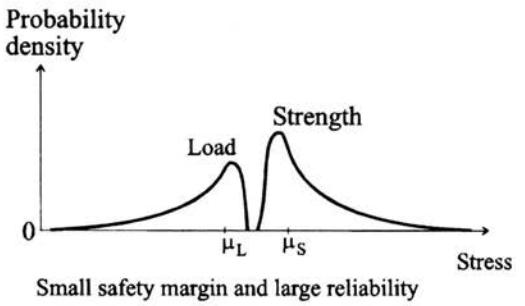

FIGURE 23.

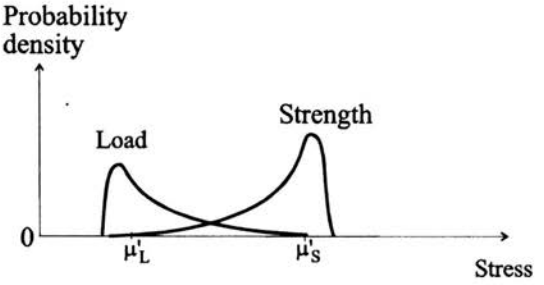

FIGURE 24.

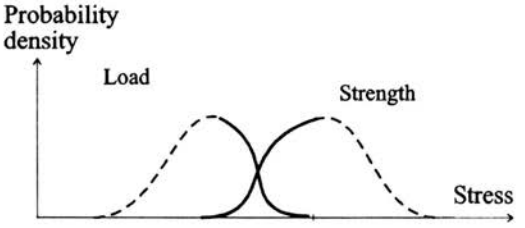

FIGURE 25.

with the distributions in Fig. 23. This example shows that the safety margin concept applied without considering the shape of the interacting distribution tails is completely misleading.

The discussion so far shows that the most important aspect of the load-strength interaction is the interaction of the upper tail of the load distribution with the lower tail of the strength distribution (Fig. 25).

4.2. Approximating the lower tail of material properties monotonically dependent on the amount of the intercepted fraction from one of the microstructural constituents

Efficient probability bounds of the property values can be obtained in the case where the property y is solely determined by the amount of the intercepted quantity from one of the constituents (e.g. density). In this case, the property value y can be expressed by a functional relationship $y(x)$ between the property value y (e.g. density, yield strength) and the intercept x from one of the structural constituents. Despite the fact that the functional relationship between the property value y and the intercept x is usually unknown, it can be shown that provided that $y(x)$ is monotonic, efficient probability bounds can be constructed regarding the property under certain conditions. The probability bounds are determined using precise estimates of the expected order statistics of the intercepts and approximate estimates of the expected order statistics of the property, obtained from a relatively small number of data sets. The expected order statistics of the intercepts can for example be obtained by sampling images of the microstructure.

Assume that estimates $\bar{y}_1 < \bar{y}_2 < \ldots < \bar{y}_n$ of the n expected order statistics of the property are available from m ordered data sets (each consisting of n measurements/samples).

Each value $\bar{y}_r$ is an average $\bar{y}_r = \frac{1}{m} \sum_{j=1}^{m} y_{j,r}$, $r = 1, n$ of the values with the same rank in the m data sets:

$$\begin{array}{llll} y_{1,1} & < y_{1,2} & < \ldots & < y_{1,n} \\ y_{2,1} & < y_{2,2} & < \ldots & < y_{2,n} \\ \ldots & \ldots & \ldots & \ldots \\ y_{m,1} & < y_{m,2} & < \ldots & < y_{m,n}. \end{array}$$

The estimates of the expected order-statistics $\bar{x}_1 < \bar{x}_2 < \ldots < \bar{x}_n$ of the intercepts are formed in a similar fashion: each value $\bar{x}_r$ is an average $\bar{x}_r = \frac{1}{Q} \sum_{j=1}^{Q} x_{j,r}$, $r = 1, n$ of the values with the same rank in Q ordered sets of intercepts ($Q \gg m$):

$$\begin{array}{llll} x_{1,1} & < x_{1,2} & < \ldots & < x_{1,n} \\ x_{2,1} & < x_{2,2} & < \ldots & < x_{2,n} \\ \ldots & \ldots & \ldots & \ldots \\ x_{Q,1} & < x_{Q,2} & < \ldots & < x_{Q,n}. \end{array}$$

Each data set of intercepts consists of n random placements (throws) of the transect in the microstructure.

It can be shown however, that if the variance of the estimated order statistic $\bar{x}_r$ of the intercepts is relatively small, the probability that the property Y will be smaller than any of its expected order statistics $\bar{y}_r$ is approximately equal to the probability that the intercept X will be smaller than the corresponding expected order statistic $\bar{x}_r$ of the intercepts, i.e:

$$P(Y \leqslant \bar{y}_r) \approx P(X \leqslant \bar{x}_r), \tag{4.3}$$

and also

$$P(\bar{y}_r \leqslant Y \leqslant \bar{y}_s) \approx P(\bar{x}_r \leqslant X \leqslant \bar{x}_s), \tag{4.4}$$

where r and s stand for the indices of any two order statistics.

If the variance of the estimated mean order statistic $\bar{x}_r$ is large however, relationships (4.3) and (4.4) are no longer valid. The bounds (4.3) and (4.4) regarding the property can be determined using the mean order statistics of the intercepts and their variances directly, from Monte Carlo simulations. The first step is to ensure by a Monte Carlo simulation that the estimated mean intercept order statistic $\bar{x}_r$ that has been selected is characterised by a small variance. If this is the case, the probability that the property Y will be smaller than the estimated mean order statistic $\bar{y}_r$ is approximately equal to the probability that the intercept will be smaller than its corresponding estimated mean order statistic $\bar{x}_r$, i.e. relationship (4.3) is valid. Accordingly, the probability that the property will lie between any two estimated order statistics $\bar{y}_r$ and $\bar{y}_s$ whose corresponding intercept order statistics $\bar{x}_r$ and $\bar{x}_s$ are characterised by small variances, can be determined from relationship (4.4).

The order statistics in the right hand side of Eqs. (4.3) and (4.4) can be estimated precisely by Monte Carlo simulations as described earlier. Unlike collecting data sets regarding the property values, collecting data sets regarding the order statistics of the intercepts is 'cheaper'. The number of data sets Q used to estimate the order statistics of the intercepts, can be much larger than the number m of data sets used to estimate the expected order statistics $\bar{y}_r$ of the property. As a result, the expected order statistics of the intercepts can be estimated very precisely.

In order to estimate the probability bound in Eq. (4.3) for example, the number N_r of random placements of the transect for which the intercept is smaller than $\bar{x}_r$ is divided to the total number N of random placements of the transect: $P(Y \leqslant \bar{y}_r) \approx P(X \leqslant \bar{x}_r) = N_r/N$.

4.3. A numerical example

The image of the microstructural cross section in Fig. 10 was sampled by line transects of length 40 units. [The longer side of the microstructural sec-

tion contains 640 length units]. The values of the property X characterising the pure microstructural constituents α and β were assumed to be $y_\beta = 10$ and $y_\alpha = 60$, respectively. With increasing the intercept $x = L_\alpha/L$ from the microstructural constituent α, the property y was assumed to increase according to the exemplary non-linear dependence:

$$y = y_\beta + (y_\alpha - y_\beta)x^2. \tag{4.5}$$

The mean order statistics of the intercepts and the property were determined for different numbers n of order statistics.

For a single order statistic ($n = 1$) the expected value of the intercept order statistic and the property order statistic are in fact the means of the intercept and property values, respectively. The simulation yielded $\bar{x}_1 = 0.6058$ for the mean of the intercepts with variance 0.041 and $\bar{y}_1 = 30.41$ for the mean of the property. As can be seen, due to the non-linear dependence (4.5) and the large variance (0.041) of the mean of the intercept, no reliable predictions from Eq. (4.2) can be made. For $n = 10$ order statistics, and for the same non-linear relationship (4.5), the corresponding expected order statistics of the intercepts calculated from the Monte Carlo simulation are given in Table 1.

TABLE 1. Mean order statistics of the intercepts x from the α-constituent from data sets each containing $n = 10$ measurements. The order statistics were calculated from a Monte Carlo simulation.

	1	2	3	4	5	6	7	8	9	10
x	0.279	0.412	0.486	0.538	0.584	0.629	0.678	0.737	0.807	0.908

Suppose that the relationship property-intercept $y(x)$ is unknown and only four data sets are available, each containing ten measurements of the property. The estimated mean order statistics of the property from four data sets only are given in Table 2.

TABLE 2. Estimated mean order statistics $\bar{y}_i$ of the property y from $m = 4$ data sets, each containing $n = 10$ measurements.

$\bar{y}_1$	$\bar{y}_2$	$\bar{y}_3$	$\bar{y}_4$	$\bar{y}_5$	$\bar{y}_6$	$\bar{y}_7$	$\bar{y}_8$	$\bar{y}_9$	$\bar{y}_{10}$
15.04	20.83	23.64	25.25	26.81	29.31	32.72	37.51	47.17	48.62

Although the actual property-intercept relationship $y(x)$ is unknown, the probability that the property will be smaller than its sixth order statistics ($\hat{y}_6 = 29.31$) for example, can be estimated easily because the Monte Carlo

simulation showed that the sixth order statistic of the intercepts is characterised by a small variance (0.0057). The probability that the property will be smaller than its sixth estimated mean order statistic is approximately equal to the probability that the intercept will be smaller than its sixth expected order statistic:

$$P(Y \leqslant \bar{y}_6) \approx P(X \leqslant \bar{x}_6). \tag{4.6}$$

Estimating the probability $P(X \leqslant \bar{x}_6)$ in the right hand side of Eq. (4.6) by a Monte Carlo simulation gives $P(X \leqslant \bar{x}_6) = 0.53$ and the probability bound for the property becomes $P(Y \leqslant \bar{y}_6) \approx 0.53$. The true probability estimated by a Monte Carlo simulation (now using the non-linear dependence (4.5)) is $P(Y \leqslant \bar{y}_6) = 0.55$. In a similar fashion, other probability bounds can be estimated, e.g. $P(Y \leqslant \bar{y}_r)$ and $P(\bar{y}_r \leqslant Y \leqslant \bar{y}_s)$, as long as the corresponding $\bar{x}_r$ and $\bar{x}_s$ are characterised by small variances. The variance of the tenth order statistics of the intercepts however (0.048) is too large and no reliable predictions can be made from Eq. (4.4).

Simulated sampling of microstructural images by transects is a powerful method to build the lower tail of properties distributions strongly dependent on the amount of intercepted fraction from one of the structural constituents. One of the advantages of the method is that the probability bounds of the property are determined without prior knowledge of the functional relationship between the property and the intercepts from the structural constituents. A large number of properties vary monotonically with the intercept from one of the structural constituents. The proposed model can be applied whenever the investigated property depends monotonically on the intercept from one of the structural constituents, provided that the selected order statistic of the intercepts is characterised by a small variance. No assumptions of a probability distribution function regarding the property are needed, which is a significant advantage compared to other methods.

The method can even be applied for single-phase microstructures whose grain-size varies substantially (inhomogeneous in terms of a grain size distribution). If the investigated property is a monotonic function of the grain size, the proposed method can be applied.

Suppose that the investigated property depends monotonically on the number of intercepted grains W by transect. Then if the estimates $\bar{w}_1 < \bar{w}_2 < \ldots$ of the mean order statistics of the number of intercepted grains are build and also the corresponding estimates $\bar{y}_1 < \bar{y}_2 < \ldots$ of the mean order statistics of the investigated property, Eqs. (4.2) and (4.4) will be valid if the estimated mean order statistics of the number of intercepted grains are characterised by small variances. The probability $P(Y \leqslant \bar{y}_r)$ that the property will be smaller than its r-th estimated mean order statistic $\bar{y}_r$

is approximately equal to the probability that the number of intercepted grains W will be smaller than its r-th estimated mean order statistic $\bar{w}_r$: $P(Y \leqslant \bar{y}_r) \approx P(W \leqslant \bar{w}_r)$.

5. Modelling the uncertainty associated with mechanical properties of inhomogeneous microstructures

5.1. Modelling uncertainty of mechanical properties using mixture distributions

A typical inhomogeneous microstructure is the microstructure of C-Mn multi-run welds (Fig. 26).

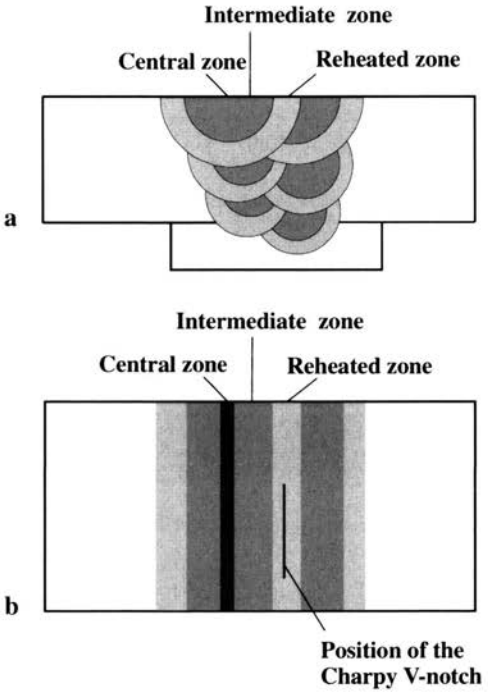

FIGURE 26.

It consists of a central zone, characterised by a poor impact toughness, reheated zone characterised by a relatively high impact toughness and an intermediate zone, characterised by an intermediate impact toughness. Each subsequent weld bead, grain refines (normalises) part of the previous weld metal underneath (Easterling, 1983) and refinements in microstructure result in improved toughness compared to the microstructure not affected by reheating. For a Charpy V-notch positioned entirely in a specific microstructural zone,

the measured impact energy will also be influenced by the other microstructural zones. Despite this dependence however, the specific microstructural zone in which the Charpy V-notch has been cut has a crucial influence on the distribution of the impact energy [67]. At each Charpy test, the notch on the specimen is parallel to the weld beads and resides entirely in a single microstructural zone (Fig. 26). The strong influence of the microstructural zone where the notch is located is illustrated by the well separated distinct empirical cumulative distributions of the impact energy characterising each zone (Fig. 27).

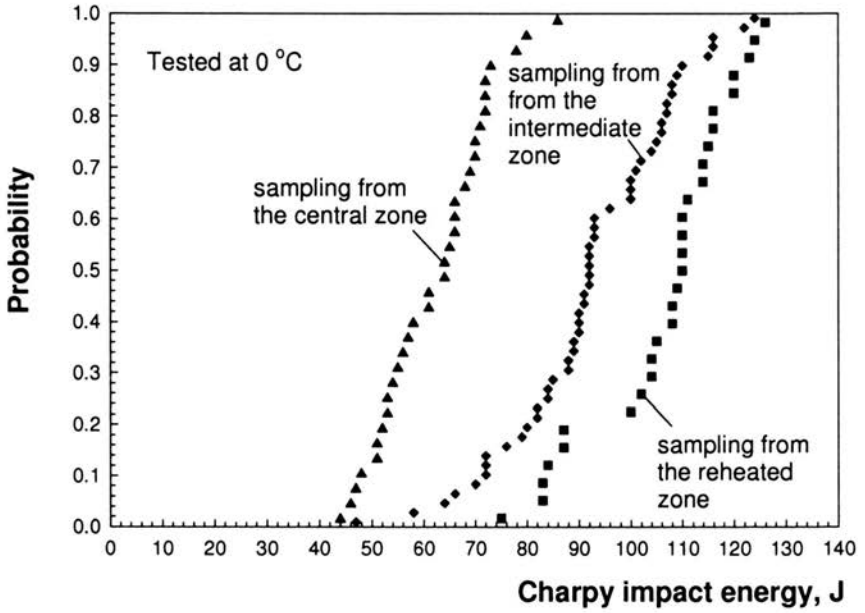

FIGURE 27.

Suppose that M microstructural zones ($i = 1, M$) are sampled by a transect with probabilities $p_1, p_2, \ldots, p_M$, $\sum_{i=1}^{M} p_i = 1$. It is assumed that a single microstructural zone is sampled at any placement of the transect. Thus, the probability $F(x) \equiv P(X \leqslant x)$ that the mechanical property X(e.g. Charpy impact energy), will be smaller or equal than a specified value x can be presented as an union of the following mutually exclusive and exhaustive events: (i) the first microstructural zone is sampled and the property is smaller than x (the probability of this compound event is given by $p_1 F_1(x)$); (ii) the second microstructural zone is sampled and the property is smaller than x (the probability of this compound event is given by $p_2 F_2(x)$);...; the M-th

microstructural zone is sampled and the property is smaller than x (the probability of this compound event is given by $p_M F_M(x)$). The probability of an union of mutually exclusive events is equal to the sum of the probabilities of the separate events and as a result:

$$F(x) = \sum_{k=1}^{M} p_k F_k(x). \tag{5.1}$$

As a result, the probability distribution $F(x) = P(X \leqslant x)$ of the mechanical property X is a mixture of the probability distribution functions $F_k(x)$ characterising the individual microstructural zones, scaled by the probabilities p_k, $k = 1, M$ with which they are sampled, where $\sum_{k=1}^{M} p_k = 1$. After differentiating Eq.(5.1), a relationship between the probability densities is obtained:

$$f(x) = \sum_{k=1}^{M} p_k f_k(x). \tag{5.2}$$

Multiplying both sides of Eq.(5.2) by x and integrating:

$$\int_{-\infty}^{+\infty} x f(x) dx = \sum_{k=1}^{M} p_k \int_{-\infty}^{+\infty} x f_k(x) dx$$

gives

$$\mu = \sum_{k=1}^{M} p_k \mu_k. \tag{5.3}$$

It must be pointed out that assumptions of a random distribution of the property can probably be justified only in cases where the same (relatively homogeneous) microstructural zone is sampled. Numerous normal probability plots of Charpy impact energy data related to the case where the Charpy V-notch samples different microstructural zones have been produced in [67]. The systematic deviations of the plotted data from a straight line demonstrated that the impact energy distribution at a specified test temperature for multi-run welds is not described by a normal (Gaussian) model.

The variance V of the mixture distribution (5.2) for continuous probability density functions $f_k(x)$ characterising the existing microstructural con-

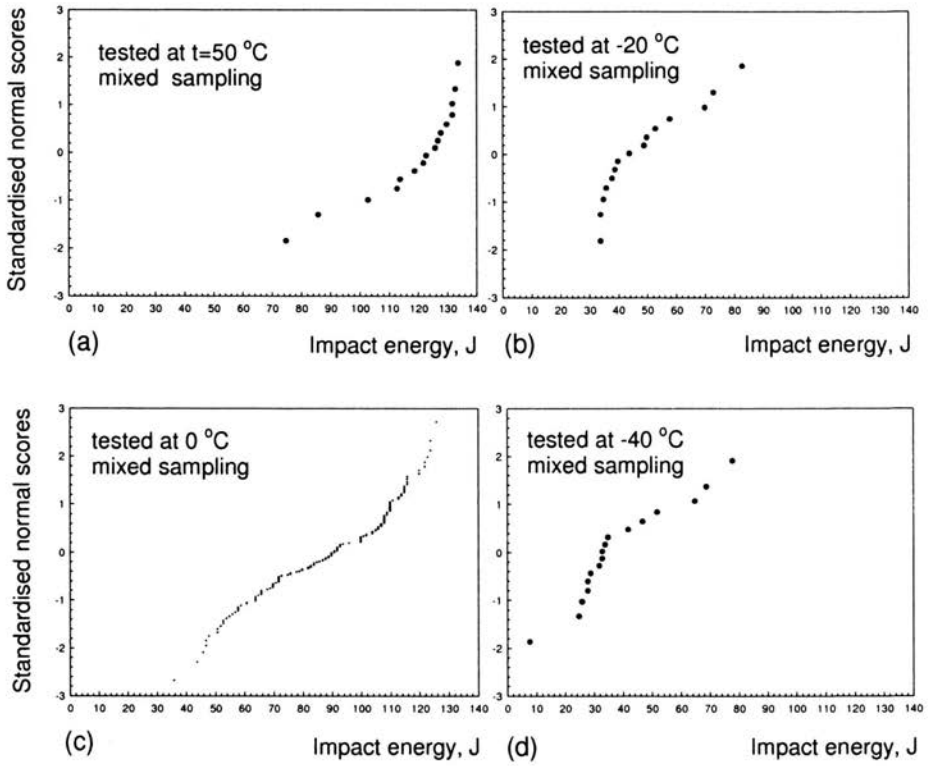

FIGURE 28.

stituents can be derived as follows

$$V = \int (x-\mu)^2 f(x)dx = \int (x-\mu_k+\mu_k-\mu)^2 \sum_{k=1}^{M} p_k f_k(x)dx =$$

$$= \sum_{k=1}^{M} p_k \left(\int (x-\mu_k)^2 f_k(x)dx + \int 2(x-\mu_k)(\mu_k-\mu) f_k(x)dx \right.$$

$$\left. + \int (\mu_k-\mu)^2 f_k(x)dx \right).$$

Because the middle integral in the expansion is zero:

$$\int 2(x-\mu_k)(\mu_k-\mu) f_k(x)dx = 0,$$

the expression for the variance becomes:

$$V = \sum_{k=1}^{M} p_k [V_k + (\mu_k-\mu)^2], \tag{5.4}$$

where V_k, $k = 1, M$ are the variances characterising the M individual distributions. Although Eq. (5.4) has a simple form, the grand mean of the distribution mixture μ given by Eq.(5.3) is a function of the means μ_k of the individual distributions. An expression for the variance can be derived as a function only of the pairwise differences between the means μ_k of the individual distributions. Indeed, substituting expression (5.3) for the mean of a distribution mixture into the term $\sum_{k=1}^{M} p_k(\mu_k - \mu)^2$ of Eq. (5.4) gives

$$\sum_{k=1}^{M} p_k(\mu_k - \mu)^2 = \sum_{k=1}^{M} p_k\mu_k^2 - \left(\sum_{k=1}^{M} p_k\mu_k\right)^2. \tag{5.5}$$

The variance of the distribution mixture can then be expressed only in terms of the pairwise differences between the means of the individual distributions. Indeed, expanding the right part of Eq. (5.5) results in:

$$\sum_{k=1}^{M} p_k\mu_k^2 - \left(\sum_{k=1}^{M} p_k\mu_k\right)^2 = p_1\mu_1^2 + p_2\mu_2^2 + \ldots + p_M\mu_M^2 - p_1^2\mu_1^2$$

$$- p_2^2\mu_2^2 - \ldots - p_M^2\mu_M^2 - 2\sum_{i=2}^{M}\sum_{j=1}^{i-1} p_ip_j\mu_i\mu_j = p_1(p_2 + p_3 + \ldots + p_M)\mu_1^2$$

$$+ p_2(p_1 + p_3 + \ldots + p_M)\mu_2^2 + \ldots + p_M(p_1 + p_2 + \ldots + p_{M-1})\mu_M^2$$

$$- 2\sum_{i<j} p_ip_j\mu_i\mu_j = \sum_{i<j} p_ip_j(\mu_i - \mu_j)^2$$

since $1 - p_1 = p_2 + p_3 + \ldots + p_M$, $1 - p_2 = p_1 + p_3 + \ldots + p_M$, etc. As a result, the variance of the distribution mixture (5.4) becomes

$$V = \sum_{k=1}^{M} p_k[V_k + (\mu_k - \mu)^2] = \sum_{k=1}^{M} p_kV_k + \sum_{i<j} p_ip_j(\mu_i - \mu_j)^2. \tag{5.6}$$

The expansion of $\sum_{i<j} p_ip_j(\mu_i - \mu_j)^2$ has $M(M-1)/2$ number of terms, equal to the number of different pairs (combinations) of indices among M indices. For $M = 2$ individual distributions, Eq. (5.6) becomes

$$V = pV_1 + (1-p)V_2 + p(1-p)(\mu_1 - \mu_2)^2. \tag{5.7}$$

For $M = 3$, Eq. (5.6) becomes

$$V = p_1V_1 + p_2V_2 + p_3V_3 + p_1p_2(\mu_1 - \mu_2)^2 + p_2p_3(\mu_2 - \mu_3)^2$$

$$+ p_1p_3(\mu_1 - \mu_3)^2. \tag{5.8}$$

Determining the variance of the distribution mixture from sampling different microstructural zones is closely related to the probability bounds of the mechanical properties associated with these zones, which is an important task of the structural reliability assessment.

Equation (5.6) does not require the type of the individual distributions to be known and has universal validity. Distribution mixtures arising from sampling inhomogeneous structural zones are characterised by large variances and this is illustrated by the box plots in Fig. 29 representing the scatter of the Charpy impact energy from sampling the individual microstructural zones and from sampling all zones.

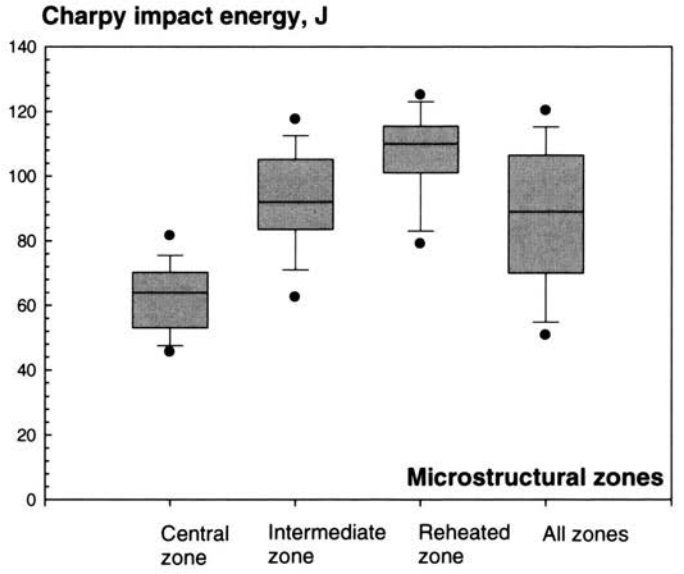

FIGURE 29.

The reason for the large variances, becomes clear from Eq. (5.6), where the variance of a distribution mixture has been decomposed into two major components. The first component $\sum_{k=1}^{M} p_k V_k$ comprises the terms $p_k V_k$, (the variances of the individual distributions characterising the separate sources) and characterises only the variation of properties *within* the separate sources (individual distributions). The second component is the sum $\sum_{i<j} p_i p_j (\mu_i - \mu_j)^2$ and characterises the variation of properties *between* the separate sources (individual distributions). Assuming that all individual distributions have the same mean $\mu (p_i = p_j = \mu)$, the terms $p_i p_j (\mu_i - \mu_j)^2$ in Eq. (5.6) become zero and the total variance becomes $V = \sum_{k=1}^{M} p_k V_k$. In other words, the total variation of the property is entirely *within-sources* variation.

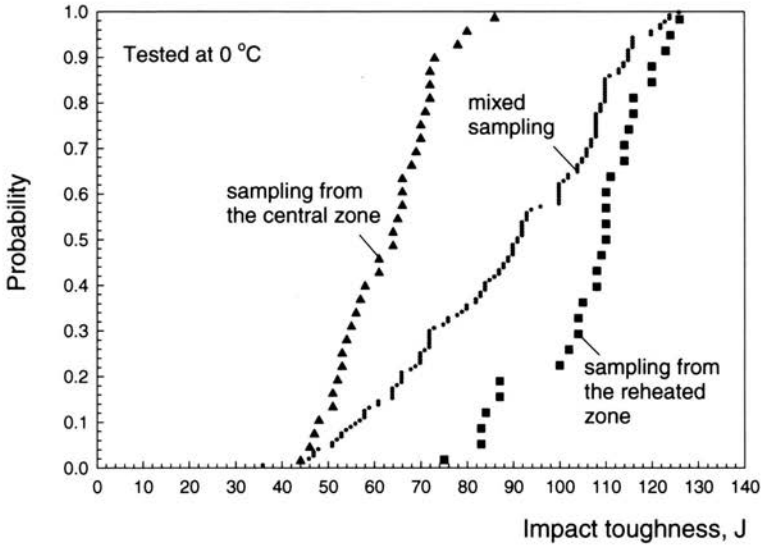

FIGURE 30.

Assuming that all sources (individual distributions) are characterised by very small variances $V_k \approx 0$, $\sum_{k=1}^{M} p_k V_k \approx 0$ and the total variance becomes $V = \sum_{i<j} p_i p_j (\mu_i - \mu_j)^2$. In other words, the total variation of the property is entirely *between-sources* variation.

5.2. Variance upper bound theorem and its applications

For the case represented in Fig. 31 where small samples are taken randomly from a three-component inhomogeneous structure (components A, B

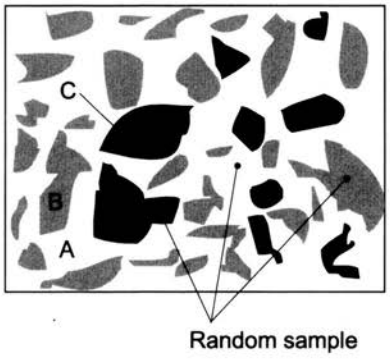

FIGURE 31.

and C) the variance of properties of the samples can be determined easily using Eq. 5.8 because the probabilities of sampling the separate microstructural constituents are equal to the volume fractions ξ_A, ξ_B and ξ_C ($p_1 = \xi_A$; $p_2 = \xi_B$; $p_3 = \xi_C$) of the microstructural constituents.

In a numerical example, suppose that the three structural constituents A, B and C have volume fractions $\xi_A = 0.55$; $\xi_B = 0.35$ and $\xi_C = 0.1$. The mean yield strength of the constituents is as follows: $\mu_A = 800\,\text{MPa}$, $\mu_B = 600\,\text{MPa}$, $\mu_C = 900\,\text{MPa}$, with standard errors $\sigma_A = 20\,\text{MPa}$; $\sigma_B = 25\,\text{MPa}$ and $\sigma_C = 10\,\text{MPa}$, correspondingly.

According to Eq. (5.8), the mean yield strength of the samples from all microstructural zones is

$$\mu = p_A\mu_A + p_B\mu_B + p_C\mu_C = 0.55 \times 800 + 0.35 \times 600 + 0.10 \times 900 = 740\,\text{MPa}$$

with a standard deviation

$$\sigma = [p_A\sigma_A^2 + p_B\sigma_B^2 + p_C\sigma_C^2 + p_Ap_B(\mu_A - \mu_B)^2 + p_Bp_C(\mu_B - \mu_C)^2 + p_Ap_C(\mu_A - \mu_C)^2]^{1/2}$$

which, after substituting the numerical values gives $\sigma \approx 108.85\,\text{MPa}$. As can be verified, the standard error characterising sampling from all microstructural constituents is significantly larger than the standard errors characterising sampling from the separate constituents.

If the mixing proportions p_k are unknown, the variance V in Eq. (5.8) cannot be calculated. Depending on the actual mixing proportions p_k, the variance V can vary from the smallest variance σ_1^2 characterising one of the constituents up to the largest possible variance obtained from sampling a particular combination of constituents with appropriate probabilities p_i. A central question is establishing a tight upper bound for the variance of properties from multiple sources (constituents) irrespective of the mixing proportions p_k characterising the sources. In order to determine a uncertainty interval for the variance of properties, the exact upper bound of the variance with respect to the probabilities of sampling p_i needs to be determined first. This can be achieved using the simple numerical algorithm in Appendix A which is based on a result of fundamental importance, derived rigorously in Appendix B:

> ***Variance upper bound theorem:*** *The exact upper bound of the variance of properties from sampling multiple microstructural constituents/sources is obtained from sampling a single or at most two microstructural constituents/sources.*

Mathematically, the upper bound variance theorem can be expressed as

$$V_{\max} = p_{\max} V_k + (1 - p_{\max}) V_l + p_{\max}(1 - p_{\max})(\mu_k - \mu_l)^2, \tag{5.9}$$

where k and l are the indices of the sources for which the maximum variance is obtained and $0 \leqslant p_{\max} \leqslant 1$ and $1 - p_{\max}$ are the probabilities of sampling the sources for which the maximum of the variance was obtained. If $p_{\max} = 1$, the maximum variance is obtained from sampling the *k-th* source only.

On the basis of this result, the algorithm for finding the maximum variance of the properties in Appendix A consists of checking the variances of all individual sources and the variances from sampling all possible pairs of sources. In this way finding the upper bound variance of the properties from M sources involves only $M(M+1)/2$ checks.

For a large M, determining the upper bound variance by finding the global maximum of expression (5.6) regarding the probabilities p_k is a difficult task.

An important application of the variance upper bound theorem will be considered here: producing conservative estimates of the uncertainty associated with material properties from sampling different microstructural zones.

5.3. A conservative estimate of the scatter of the Charpy impact energy at a specified test temperature

The methodology for determining the upper bound variance of properties from multiple sources is particularly useful in the case where the sources are microstructural zones and the mixing proportions are the probabilities with which these microstructural zones are sampled. In this way, a conservative estimate of the scatter of material properties from arbitrary sampling of the microstructural zones is obtained since, as a rule, the probabilities p_k with which these zones are sampled are *unknown*. The power of the proposed methodology will be illustrated by applying it to determine a conservative scatter interval for the Charpy impact energy of multi-run welds.

Determining the uncertainty related to the Charpy impact energy at a specified test temperature is based on experimental data published in [67] and on Eq. (5.6) related to a variance of a distribution mixture. The experimental data characterise the Charpy impact energy from sampling the central, intermediate and reheated zone [67] of multi-run *C-Mn* welds at 0°C and include 117 Charpy impact energy measurements. The impact energy of the central zone is characterised by an individual distribution with mean $\mu_1 = 62.32$ and a standard deviation $\sigma_1 = 10.49$ calculated on the basis of 34 measurements; the impact energy of the intermediate zone is characterised by an empirical distribution with mean $\mu_2 = 92.22$ and a standard deviation $\sigma_2 = 16.02$ calculated on the basis of 54 measurements and the impact energy

of the reheated zone is characterised by an empirical distribution with mean $\mu_3 = 106.22$ and a standard deviation $\sigma_3 = 13.63$ calculated on the basis of 29 measurements. For $M = 3$ microstructural zones (central, intermediate and reheated), Eq. (5.1) yields a model for the distribution of the Charpy impact energy:

$$F(x) = p_1 F_1(x) + p_2 F_2(x) + p_3 F_3(x), \tag{5.10}$$

where p_1, p_2 and p_3 are the probabilities of sampling the central (1), intermediate (2) and reheated zone (3) and $F_1(x)$, $F_2(x)$ and $F_3(x)$ are the cumulative distribution functions characterising the Charpy impact energy of the three microstructural zones.

According to Eq. (5.3) the mean of the Charpy impact energy at 0°C is given by

$$\mu = p_1\mu_1 + p_2\mu_2 + p_3\mu_3, \tag{5.11}$$

where $\mu_1 = 62.32$, $\mu_2 = 92.22$ and $\mu_3 = 106.22$ are the means of the Charpy impact energy characterising the three microstructural zones. For $M = 3$ microstructural zones equation Eq. (5.8) gives

$$V_0 = p_1\sigma_1^2 + p_2\sigma_2^2 + p_3\sigma_3^2 + p_1p_2(\mu_1 - \mu_2)^2 + p_2p_3(\mu_2 - \mu_3)^2 + p_1p_3(\mu_1 - \mu_3)^2 \tag{5.12}$$

for the variance of the Charpy impact toughness at 0°C, where $\sigma_1 = 10.49$, $\sigma_2 = 16.02$ and $\sigma_3 = 13.63$ are the standard deviations associated with the Charpy impact energy of the individual microstructural zones. Because the probabilities p_1, p_2 and p_3 of sampling the individual microstructural zones are unknown, the variance V from Eq. (5.12) cannot be calculated. Depending on the actual probabilities with which the microstructural zones are sampled, the variance V may vary from the smallest variance σ_1^2 characterising the central zone up to the largest possible variance obtained from sampling a particular combination of microstructural zones with particular probabilities p_i. In order to determine a conservative uncertainty interval for the variance, the exact upper bound of the variance needs to be determined first.

The global maximum of the variance of a distribution mixture composed by the three microstructural zones, regarding the probabilities p_i with which they are sampled is $V_{\max} \approx 492.109$. The upper bound of the variance in Eq. (5.12) has been obtained by maximising V regarding the sampling probabilities p_1, p_2 and p_3 using the numerical algorithm in Appendix A. For sampling probabilities $p_1 \approx 0.5$, $p_2 = 0$ and $p_3 = 0.5$, the numerical algorithm determined $V_{\max} \approx 492.109$ for the variance upper bound. The mean

of the distribution mixture which corresponds to the upper bound of the variance of the Charpy impact energy is $\mu = 0.5\mu_1 + 0.5\mu_3 = 84.27$. In this way, the uncertainty associated with the Charpy impact toughness at a specified test temperature (0°C) has been determined and can subsequently be used for determining the uncertainty associated with the location of the ductile-to-brittle transition region. As can be verified from Eq. (5.12), the variation associated with the Charpy impact energy at a specified test temperature is caused by the natural variability of the impact energy from sampling a particular microstructural zone and from sampling multiple microstructural zones. According to Eq. (5.12) the variation can be reduced significantly if a single microstructural zone (for example the central zone) is sampled. The probabilities of sampling then become $p_1 = 1$, $p_2 = 0$ and $p_3 = 0$ and Eq. (5.12) transforms into $V_0 = \sigma_1^2$, i.e. the variance coincides with the variance of the Charpy impact energy of the central zone. By sampling from a single microstructural zone, the variability associated with the Charpy impact energy diminishes because the squared differences $\sum_{i<j} p_i p_j (\mu_i - \mu_j)^2$ in Eq. (5.6) disappear.

5.4. Conservative estimate regarding the uncertainty in the location of the ductile-to-brittle transition region

According to the earlier discussion in Sec. 2, the largest scatter of properties associated with sampling of an inhomogeneous microstructure by a line transect corresponds to a sampling scheme characterised by the largest intercept variance. For multi-run welds this 'conservative sampling scheme' corresponds to a sampling with a Charpy V-notch parallel to the weld beads (Fig. 26(b)) which yields the largest variance of the Charpy impact energy. The Monte Carlo simulations showed that the variance of the 40 J transition

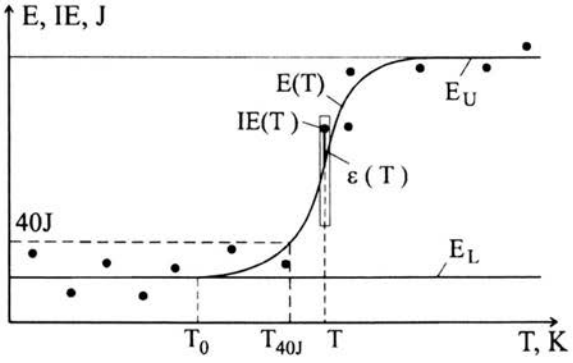

FIGURE 32.

temperature (the T40J temperature corresponding to 40 J impact energy, selected to mark the location of the transition region, Fig. 32) increases with increasing the variance of the impact energy at the test temperatures. A large scatter in the Charpy impact energy propagates into a large uncertainty in the location of the ductile-to-brittle transition region. Consequently, the conservative sampling scheme (a Charpy V-notch parallel to the weld beads, Fig. 26) can be selected as a basis for producing a conservative estimate of the uncertainty associated with the location of the ductile-to-brittle transition region.

The models for determining the uncertainty associated with the Charpy impact energy of *C-Mn* multi-run welds proposed here integrate the following basic components:

(i) A model of the systematic component of the Charpy impact energy variation [60];

(ii) A model for producing unbiased and precise estimates of the parameters of the systematic component of the Charpy impact energy in the transition region [60];

(iii) A model of the variance of the Charpy impact toughness at a specified test temperature [57];

(iv) A simulation model for determining the uncertainty associated with the location of the transition region [55] and

(v) A model for determining the uncertainty associated with the Charpy impact energy at a specified test temperature [55].

The general statistical model regarding the variation $IE(T)$ of the Charpy impact energy can be presented as

$$IE(T) = E(T) + \varepsilon(T), \tag{5.13}$$

where $E(T)$ is the systematic component of the impact energy variation and $\varepsilon(T)$ is the random component (Fig. 32). According to Eq. (5.1), the random component $\varepsilon(T)$ of the Charpy impact energy is a mixture of several individual distributions. The model of the systematic variation $E(T)$ of the Charpy impact energy combines an equation for fitting the systematic variation of the normalised impact energy and involves separate treatment of the shelf regions E_U and E_L (Fig. 32) and the transition ductile-to-brittle region (Fig. 33). A method for producing unbiased and precise estimates of the parameters in the systematic variation has been proposed in [60].

A conservative estimate of the uncertainty in the location of the ductile-to-brittle region along the temperature axis can be produced using Monte Carlo simulations based on fitting multiple sparse data sets obtained from conservative sampling. This consists of sampling the individual microstruc-

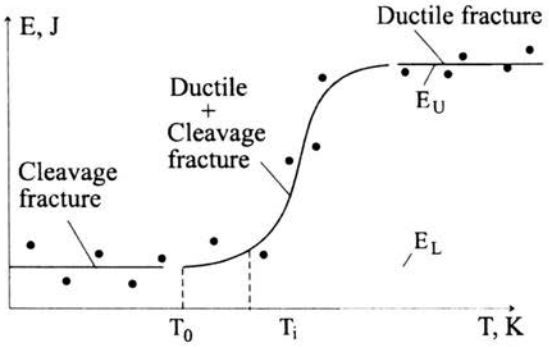

FIGURE 33.

tural constituents (at each test temperature) with probabilities which result in the largest variance of the Charpy impact energy. Correspondingly, in order to produce a conservative estimate of the location of the ductile-to-brittle transition region, at each test temperature T_i, the components in the distribution mixture modelling the Charpy impact energy is sampled with probabilities which result in the largest Charpy impact energy variance.

A uniform distribution regarding the scatter of the Charpy impact toughness at a specified test temperature is also assumed. This assumption is also conservative and is supported by the actual shape of the empirical distributions of the Charpy impact energy (Fig. 30).

The Monte Carlo simulation algorithm for producing a conservative estimate of the location of the transition region as a function of the selected test temperatures works as follows. Sequentially, the selected input test temperatures are scanned and at each test temperature, a random value the

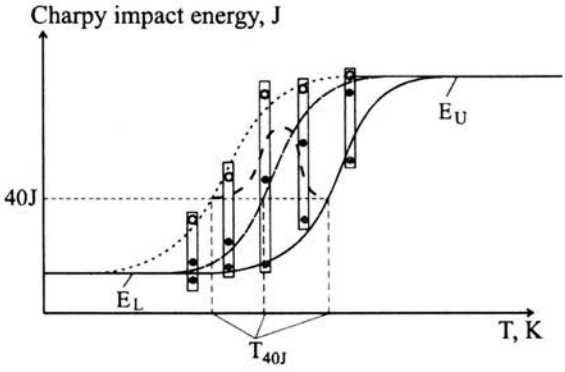

FIGURE 34.

Charpy impact energy is generated from the uncertainty interval of the impact energy at that test temperature (Fig. 34). In this way, by a single scan of all test temperatures, a random sparse data set is generated, containing a single impact energy at each test temperature. After generating a set of simulated values of the Charpy impact energy at each test temperature, the obtained sparse data set is fitted according to the method presented in [60].

Next, the T_{40J} transition temperature from fitting the sparse data set is determined (marking the location of the transition region), after which another scan of the test temperatures is performed which results in a new sparse data set. The subsequent fitting of the new sparse data set results in another estimate of the T_{40J} temperature. The Monte Carlo trials continue with generating sparse data sets, fitting the data sets and determining estimates of the T_{40J} temperature until a sufficient number of estimates are collected. These form an empirical statistical distribution, describing the uncertainty associated with the T_{40J} temperature marking the start of the ductile-to-brittle transition region (Fig. 34).

The Monte Carlo simulation routine for investigating the uncertainty associated with the location of the transition region as a function of the number of test temperatures, the choice of test temperatures and the magnitude of the variance of the impact energy at the test temperatures has been discussed in [55].

A parametric study based on real Charpy impact data at eight test temperatures ($-70°C$, $-40°C$, $-20°C$, $-10°C$, $0°C$, $10°C$, $20°C$, $50°C$) has been discussed in [55]. The histogram in Fig. 35 represents the uncertainty in the

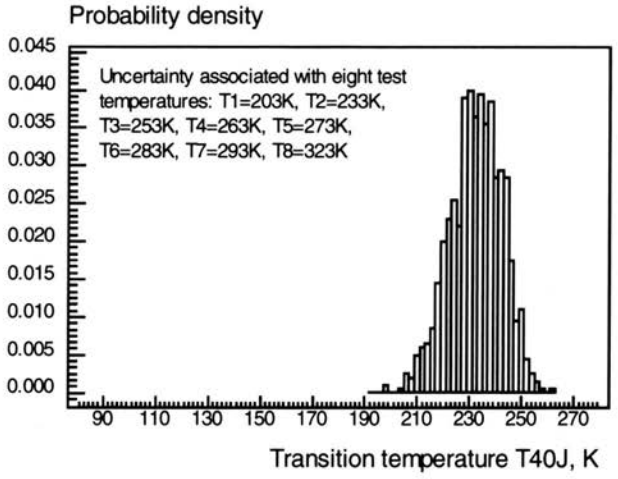

FIGURE 35.

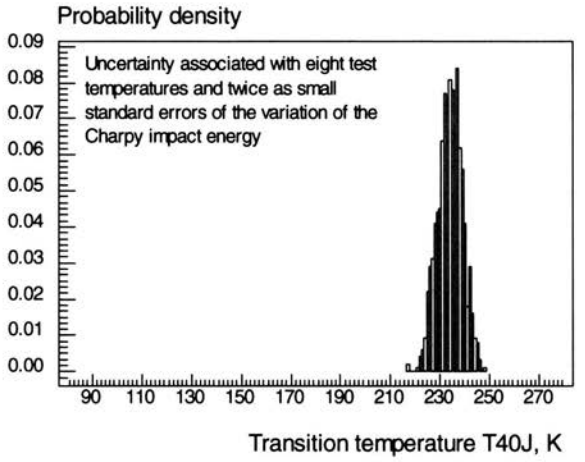

FIGURE 36.

location of the transition region associated with eight test temperatures. The histogram in Fig. 36 represent the uncertainty in the location of the transition region for the same eight test temperatures but with twice as small standard errors of the variation of the Charpy impact energy. As can be verified from the histograms, decreasing the uncertainty intervals of the Charpy impact energy at the test temperatures significantly diminishes the uncertainty associated with the location of the transition region.

The uncertainty in the location of the ductile-to-brittle transition region depends very strongly on the number of test temperatures and the variance of the impact energy at the test temperatures. The large uncertainty in the Charpy impact energy from sampling more than one microstructural zone combined with a small number of test temperatures propagates into a large uncertainty in the location of the ductile-to-brittle transition region. For a specified number of test temperatures, the uncertainty in the location of the transition region can be reduced by sampling a single microstructural zone. Sampling from the central zone only for example, results in a conservative estimate of the location of the transition region, shifted towards higher temperatures.

Appendix A. An algorithm in pseudo-code for determining the upper bound of the variance from sampling from multiple sources

The variable `max` contains the maximum variance at the end of the calculations, the constant `M` is the number of components (sources) composing

the mixture distribution. Variables k_max and m_max contain the indices of the two sources sampling from which yields the largest variance. If the maximum variance is attained at sampling a single source, k_max and m_max will both contain the index of this source. Variables pk_max and pm_max contain the probabilities of sampling the two sources which have produced the largest variance. The operators in braces $\{op1;\ op2;\ op3;\ldots;\}$ are executed as a single block. As can be verified the internal loop is executed only if the condition $|V[i] - V[j]| < (\mu[i] - \mu[j])^2$ is fulfilled, i.e. only if a local maximum from sampling the two sources exists.

```
max=V[1]; k_max=1; m_max=1;
for i from 2 to M do
 {
  if (max<V[i]) then do
   {
    max=V[i]; k_max=i;
    m_max=i; pk_max=1; pm_max=1;
   }
  for j=1 to i do
   {
    if |V[i] − V[j]| < (μ[i] − μ[j])^2 then do
     {
      candidate_max=V[i]/2+V[j]/2+(V[i]-V[j])^2/(4(μ[i]−μ[j])^2)+((μ[i]−μ[j])/2)^2
      if (max < candidate_max) then do
       {
        max=candidate_max; k_max=i; m_max=j;
        pk_max = 0.5 + (V[i]−V[j])/(2(μ[i]−μ[j])^2);
        pm_max=1-pk_max;
       }
     }
   }
```

Appendix B.

The upper bound $V_{\max}$ of the variance V of a distribution mixture is obtained by maximising the general Eq. (5.6) regarding p_k, $k = 1, M$:

$$V_{\max} = \max_{p_1 p_2 \ldots p_M} \left(\sum_{k=1}^{M} p_k V_k + \sum_{i<j} p_i p_j (\mu_i - \mu_j)^2 \right). \tag{B.1}$$

The local extrema of expression (B.1) can be found using Lagrange multipliers, because of the equality constraint: $g(p_1, \ldots, p_M) \equiv \left(\sum_{k=1}^{M} p_k\right) - 1 = 0$. The necessary condition for an extremum of the variance given by expression (5.6) is:

$$\partial V/\partial p_k + \lambda \partial g/\partial p_k = 0, \quad k = 1, 2, \ldots, M, \tag{B.2}$$

where λ is the Lagrange multiplier. These M equations together with the constraint $\sum_{k=1}^{M} p_k - 1 = 0$ form a system of $M + 1$ linear equations in the $M + 1$ unknowns $p_1, \ldots, p_M$ and λ:

$$\begin{aligned} p_1 + p_2 + \ldots + p_M &= 1, \\ \lambda + p_1(\mu_k - \mu_1)^2 + p_2(\mu_k - \mu_2)^2 + \ldots + p_{k-1}(\mu_k - \mu_{k-1})^2 & \\ + p_{k+1}(\mu_k - \mu_{k+1})^2 + \ldots + p_M(\mu_k - \mu_M)^2 &= -V_k, \end{aligned}$$

where $k = 1, M$. This linear system can also be presented in a vector form:

$$\mathbf{Ap} = \mathbf{V}, \tag{B.3}$$

where

$$\mathbf{A} = \begin{pmatrix} 0 & 1 & 1 & 1 & 1 \\ 1 & 0 & (\mu_1 - \mu_2)^2 & \ldots & (\mu_1 - \mu_M)^2 \\ 1 & (\mu_2 - \mu_1)^2 & 0 & \ldots & (\mu_2 - \mu_M)^2 \\ \ldots & \ldots & \ldots & \ldots & \ldots \\ 1 & (\mu_M - \mu_1)^2 & (\mu_M - \mu_2)^2 & \ldots & 0 \end{pmatrix},$$

$$\mathbf{p} = \begin{pmatrix} \lambda \\ p_1 \\ p_2 \\ \ldots \\ p_M \end{pmatrix}, \quad \text{and} \quad \mathbf{V} = \begin{pmatrix} 1 \\ -V_1 \\ -V_2 \\ \ldots \\ -V_M \end{pmatrix}. \tag{B.4}$$

Matrix $\mathbf{A}$ is a Cayley-Menger matrix (Glitzmann and Klee, 1994). The determinant of this matrix is at the basis of a method for calculating the volume V of a N-simplex (in the N-dimensional space). Suppose an N-simplex has vertices $v_1, v_2, \ldots, v_{N+1}$ and d_{km}^2 is the squared distance between vertices v_k and v_m. Let the matrix $\mathbf{A}$ of $\mathbf{D} = (d_{km})$ be defined as

$$\mathbf{A} = \begin{pmatrix} 0 & 1 & \ldots & 1 \\ 1 & d_{11}^2 & \ldots & d_{1,N+1}^2 \\ \ldots & \ldots & \ldots & \ldots \\ 1 & d_{N+1,1}^2 & \ldots & d_{N+1,N+1}^2 \end{pmatrix}.$$

The equation $V^2 = \frac{(-1)^{N+1}}{2^N (N!)^2} \det(\mathbf{A})$ then gives the volume V of the N-simplex (Glitzmann and Klee, 1994; Sommerville, 1958). From this equation it is clear that if the Cayley-Menger determinant is zero, the volume of the simplex is also zero. The converse is also true, if the volume of the simplex is zero, the Cayley-Menger determinant is necessarily zero.

As can be seen from our matrix $\mathbf{A}$, the means μ_i can be considered as first-axis co-ordinates of the vertices of a simplex in an $M-1$-dimensional space with other co-ordinates set to zero. The 'volume' of this simplex is clearly zero except in the one-dimensional case ($M-1=1$) where the 'volume' of the simplex is simply the distance $|\mu_1 - \mu_2|$ between the two means of the individual distributions (sources). As a consequence, the determinant of matrix A is always zero for $M > 2$ and the system (B.3) has no solution.

We will now prove that no local maximum exists if exactly $k > 2$ individual distributions (sources) are sampled from a mixture distribution composed by M components (individual distributions). If k individual distributions are sampled, the sampling probabilities of these individual distributions must then all be different from zero. Without loss of generality let us assume that the first k individual distributions are sampled with probabilities $p_1 \neq 0$; $p_2 \neq 0, \ldots, p_k \neq 0$, $\sum_{i=1}^{k} p_i = 1$, $(p_{k+1} = 0, \ldots, p_M = 0)$. Since the k individual distributions also form a mixture distribution and $k > 2$, the linear system (B.3) has no solution, therefore no local maximum exists. This means that the global maximum is attained somewhere on the boundary of the domain $0 \leqslant p_1 \leqslant 1, \ldots, 0 \leqslant p_k \leqslant 1$, either for some $p_s = 0$ or for some $p_t = 1$. The relationship $p_t = 1$ however, means that the rest of the sampling probabilities must be zero ($p_i = 0$ for $i \neq t$). In both cases, at least one of the sampling probabilities $p_1, p_2, \ldots, p_k$ must be zero. If $k = 2$ (one dimensional simplex), the matrix Eq. (B.3) becomes

$$\begin{pmatrix} 0 & 1 & 1 \\ 1 & 0 & (\mu_1 - \mu_2)^2 \\ 1 & (\mu_1 - \mu_2)^2 & 0 \end{pmatrix} \times \begin{pmatrix} \lambda \\ p_1 \\ p_2 \end{pmatrix} = \begin{pmatrix} 1 \\ -V_1 \\ -V_2 \end{pmatrix}. \tag{B.5}$$

Because in this case, the Cayley-Menger determinant is equal to $2(\mu_1 - \mu_2)^2$, a solution of the linear system (B.5) now exists and a local maximum may be present. The solution of the linear system (B.5) is

$$p_1 = 0.5 + \frac{V_1 - V_2}{2(\mu_1 - \mu_2)^2}, \tag{B.6}$$

$$p_2 = 0.5 - \frac{V_1 - V_2}{2(\mu_1 - \mu_2)^2}. \tag{B.7}$$

These values of p_1 and p_2 correspond to a local maximum in the domain $0 \leqslant p_1 \leqslant 1, 0 \leqslant p_2 \leqslant 1$, only if $|V_1 - V_2| < (\mu_1 - \mu_2)^2$. If $|V_1 - V_2| \geqslant (\mu_1 - \mu_2)^2$, the maximum is attained at the boundary points of the domain, either for $p_1 = 1$, $p_2 = 0$ ($V_{\max} = V_1$) or for $p_1 = 0$, $p_2 = 1$ ($V_{\max} = V_2$), whichever is greater ($V_{\max} = \max\{V_1, V_2\}$). If $|V_1 - V_2| < (\mu_1 - \mu_2)^2$, a local maximum of the variance exists for p_1 and p_2 given by the relationships (B.6) and (B.7). The maximum value of the variance corresponding to these values is

$$V_{\max} = \frac{V_1 + V_2}{2} + \frac{(V_1 - V_2)^2}{4(\mu_1 - \mu_2)^2} + \left(\frac{\mu_1 - \mu_2}{2}\right)^2. \tag{B.8}$$

In short, the global maximum of the right hand side of Eq. (B.3) is attained either from sampling a single source/individual distribution, in which case one of the sampling probabilities p_i is unity and the rest are zero ($p_i = 1$; $p_{j \neq i} = 0$), or from sampling only two individual distributions k and m among all individual distributions composing the mixture distribution. In this case, $p_k \neq 0$ and $p_m \neq 0$ and the rest of the p_i are zero ($p_i = 0$) for $i \neq k$ and $i \neq m$. If $V_{\max,k,m}$ denotes the local maximum of the variance from sampling sources/individual distributions k and m ($k \neq m$), the global maximum $V_{\max}$ of the right hand side of Eq. (B.3) can be presented as $V_{\max} = \max\{V_1, V_2, \ldots, V_M, V_{\max,k,m}\}$ where $k = 2, M$ and $m = 1, k-1$. Since there exist $M \times (M-1)/2$ possible terms $V_{\max,k,m}$, the global maximum is determined after $M + M \times (M-1)/2 = M(M+1)/2$ checks. As can be verified from the algorithm presented in Appendix 5A, the maximum of the variance is determined by two nested loops. The control variable `i` of the external loop takes on values from 2 to M (the number of sources) while the control variable `j` of the internal loop takes on values from 1 to `i-1`.

References

1. American Society for Metals, Metals Handbook Vol.9: *Metallography and Microstructures*, 1985.
2. K.E. Atkinson, *An Introduction to Numerical Analysis*, 2nd ed., Wiley, 1989.
3. M. Avrami, *J. Chem. Phys.*, Vol.7(1103), 1939; Vol.8(212), 1940; Vol.9(177), 1941.
4. R.E. Barlow and F. Proschan, *Statistical Theory of Reliability and Life Testing*, Holt, Rinehart and Winston, Inc., New York, 1975.
5. S.B. Batdorf and J.G. Crose, *J. Applied Mechanics*, pp.459-464, 1974.
6. I.F. Blake, *An Introduction to Applied Probability*, John Wiley & Sons, 1979.
7. A.D.C. Carter, *Mechanical Reliability*, Macmillan Education Ltd., 1986.
8. F. Chayes, *Petrographic Modal Analysis*, John Wiley & Sons Inc., New York, 1956.

9. J.W. CHRISTIAN, *The Theory of Transformations in Metals and Alloys*, Pergamon Press, Oxford, 1965.

10. P. CHRISTENSEN and M. BAKER, *Structural Reliability Theory and its Applications*, Springer-Verlag, Berlin, 1982.

11. H.A. DAVID, *Order Statistics*, 2nd Ed., John Wiley & Sons, Inc., New York, 1981.

12. M. DEGROOT, *Probability and Statistics*, Addison-Wesley, 1989.

13. E. EASTERLING, *Introduction to the Physical Metallurgy of Welding*, Butterworths, 1983.

14. A.G. EVANS, *Journal of the American Ceramic Society*, Vol.61, pp.302-308, 1978.

15. B.S. EVERITT and D.J. HAND, *Finite Mixture Distributions*, Chapman and Hall, London, 1981.

16. H.L. EWALDS and R.J.H. WANHILL, *Fracture Mechanics*, Edward Arnold, London, 1989.

17. A.M. FREUDENTHAL, Safety and the probability of structural failure, *American Society of Civil Engineers Transactions*, paper No.2843, pp.1337-1397, 1954.

18. R.L FULLMAN, Measurement of particle sizes in opaque bodies, *Transactions AIME, Journal of metals*, pp.447-452, 1953.

19. A. GLAGOLEV, Quantitative analysis with the microscope by the point method, *Eng. Min. J.*, Vol.135, pp.399, 1934.

20. P. GLITZMANN, and V. KLEE, Polytopes: 'On some Complexity of some basic problems in computational convexity II. Volume and mixed volumes'. In: *Polytopes: Abstract, Convex and Computational*, T. Bisztriczky et al. (Eds.), Dordrecht, Kluwer, 1994.

21. B.V. GNEDENKO, *The Theory of Probability*, Chelsea Publishing Company, 1962.

22. A.M. GOKHALE and W.J. DRURY, Efficient Measurement of microstructural surface area using trisector, *Metallurgical and Materials Transactions A*, Vol.25A, pp.919-928, 1994.

23. H.J.G. GUNDERSEN and E.B. JENSEN, The efficiency of systematic sampling in stereology and its prediction, *Journal of Microscopy*, Vol.147, pp.229-263, 1987.

24. D. HEARN and M.P. BAKER, *Computer Graphics: C Version*, Prentice Hall Inc., 1997.

25. E.J. HENLEY and KUMAMOTO, *Reliability Engineering and Risk Assessment*, Prentice-Hall Inc, 1981.

26. J.E. HILLIARD, Measurement of volume in volume, in: *Quantitative Microscopy*, R.T. DeHoff and F.N. Rhines (Eds.), McGraw-Hill Inc, pp.45-76, 1968.

27. J.E. HILLIARD and J.W. CAHN, An evaluation of procedures in quantitative metallography for volume-fraction analysis, *Transactions of the Metallurgical Society of AIME*, Vol.221, pp.344-352, 1961.

28. J.D. FOLEY, A. VAN DAM, S.K. FEINER, and J.F. HUGHES, *Computer Graphics: Principles and Practice*, Addison-Wesley Publishing Company, 1996.

29. W.A. JOHNSON and R.F. MEHL, *Trans. Am. Inst. Min. Metall. Engrs* Vol.135, 416, 1939.

30. D.C. KAY, *Graphics File Formats*, 2nd ed., Windcrest/McGraw-Hill, 1995.

31. M.G. KENDALL and P.A.P. MORAN, *Geometrical Probability*, Charles Griffin & Company Ltd., London, 1963.

32. A.N. KOLMOGOROV, *Izv. Akad. Nauk. SSSR.* Vol.3, 355, 1937.

33. B. LU and S. TORQUATO, Lineal-path function for random heterogeneous materials, *Physical Review A*, Vol.45, No.2, pp.922-929, 1992.

34. B. LU and S. TORQUATO Lineal-path function for random heterogeneous materials. II. Effect of polydispersity, *Physical Review A*, Vol.45, No.10, pp.7292-7301, 1992.

35. B. LU and S. TORQUATO Nearest-surface distribution functions for polydispersed particle systems, *P*hysical Review A, Vol.45, No.8, pp.5530-5544, 1992.

36. B. LU and S. TORQUATO Chord-length and free-path distribution functions for many-body systems, *Journal of Chemical Physics*, Vol.98, No.8, pp.6473-6482, 1993.

37. I. MILLER and M. MILLER, *John E.Freund's Mathematical Statistics*, 6th ed. Prentice Hall International, Inc., New York, 1999.

38. D.C. MONTGOMERY, G.C. RUNGER and N.F. HUBELE, *Engineering Statistics*, 2nd ed., John Wiley & sons, New York, 2001.

39. S.K. PARK and K.W. MILLER, Random number generators: Good ones are hard to find, *Communications of the ACM*, Vol.31, No.10, 1988.

40. PARZEN, *Modern Theory of Probability and its Applications*, John Wiley & Sons, Inc., New York, 1960.

41. J.A. RICE, *Mathematical Statistics and Data Analysis*, 2nd Ed., Duxbury Press, California, 1995.

42. S. RIMMER, *Bit-Mapped Graphics*, 2nd ed., Windcrest/McGraw-Hill, 1993.

43. A. ROSIWAL, Ueber geometrische Gesteinsanalysen usw., *Verh. der k.k. Geolog. Reichsanstalt Wien*, pp.143-175, 1898.

44. S.M. ROSS, *Introduction to Probability Models*, 7th ed. A Harcourt Science and Technology Company, 2000.

45. R.Y. RUBINSTEIN, *Simulation and the Monte-Carlo Method*, John Wiley & Sons, New York, 1986.

46. C. SAINTE CATHERINE, H. CARIUS and M. DI FANT, *Fatigue Fract. Engng Mater. Struct.* Vol.18, pp.597-604, 1995.

47. SALTYKOV, *Stereometric Metallography* , 2nd ed., Metallurgizdat, Moscow, 1958.

48. I.M. SOBOL, *A Primer for the Monte-Carlo method*, CRC Press, Boca Raton, 1994.

49. D.M.Y. SOMMERVILLE, *An introduction to the Geometry of N Dimensions*, New York, Dover, 1958.

50. H. TEICHER, Identifiability of finite mixtures, *The Annals of Mathematical Statistics* Vol.34, pp.1265-1269, 1963.

51. W.A. THOMPSON, *Point Process Models with Applications to Safety and Reliability*, Chapman & Hall, New York, 1988.

52. D.M. TITTERINGTON, A.F.M. SMITH, U.E. MAKOV, *Statistical Analysis of Finite Mixture Distributions*, Chichester, John Wiley & Sons, 1985.

53. M.T. TODINOV, Statistics of inhomogeneous media formed by nucleation and growth, *Probabilistic Engineering Mechanics*, Vol.18, pp.139-149, 2003.

54. M.T. TODINOV, Modelling consequences from failure and material properties by distribution mixtures, *Nuclear Engineering and Design*, Vol.224, pp.233-244, 2003.

55. M.T. TODINOV, Uncertainties and risk associated with the Charpy impact toughness of multi-run C-Mn welds, *Proceedings of the UNCERT-AM Conference*, A.S. Jovanovic (Ed.), published by MPA Stuttgart, 2003.

56. M.T. TODINOV, On Coolen's comments related to statistics of defects in one-dimensional components, *Computational Materials Science*, Vol.29, pp.253-258, 2004.

57. M.T. TODINOV, Distribution mixtures from sampling of inhomogeneous microstructures: variance and probability bounds of the properties, *Nuclear Engineering and Design*, Vol.214, pp.195-204, 2002.

58. M.T. TODINOV, Statistics of defects in one-dimensional components, *Computational Materials Science*, Vol.24, pp.430-442, 2002.

59. M.T. TODINOV, Distribution of properties from sampling inhomogeneous materials by line transects, *Probabilistic Engineering Mechanics*, Vol.17 pp.131-141, 2002.

60. M.T. TODINOV, An efficient method for estimating from sparse data the parameters of the impact energy variation in the ductile-to-brittle transition region, *International Journal of Fracture*, Vol.111, pp.131-150, 2002.

61. M.T. TODINOV, Statistical modelling of the scatter of properties from sampling of inhomogeneous materials, *Computational Materials Science*, Vol.21, pp.436-451, 2001.

62. M.T. TODINOV Estimating the probabilities of triggering brittle fracture associated with the defects in the materials, *Materials Science and Engineering A*, Vol.302, No.2, pp.235-245, 2001.

63. M.T. TODINOV, Estimating the parameters of the impact energy variation in the ductile-brittle transition region from complete and sparse data sets, *Computational Materials Science*, Vol.21, pp.111-123, 2001.

64. M.T. TODINOV, Probability distribution of fatigue life controlled by defects, *Computers & Structures*, Vol.79, pp.313-318, 2001.

65. M.T. TODINOV, On some limitations of the Johnson-Mehl-Avrami-Kolmogorov equation, *Acta Materialia*, Vol.48, pp.4217-4224, 2000.

66. M.T. TODINOV Probability of fracture initiated by defects, *Materials Science & Engineering A*, Vol.A276, pp.39-47, 2000.

67. M.T. TODINOV, M.NOVOVIC, P.BOWEN AND J.F.KNOTT., Modelling the impact energy in the ductile/brittle transition region of C-Mn multi-run welds, *Materials Science & Engineering A*, Vol.A287, pp.116-124, 2000.

68. M.T. TODINOV, On some applications of the random transects, *Modelling and Simulation in Materials Science and Engineering*, Vol.7, pp.525-539, 1999.

69. M.T. TODINOV, A new approach to the kinetics of a phase transformation with constant radial growth rate, *Acta materialia*, Vol.44, pp.4697-4703, 1996.

70. S. TORQUATO, Random Heterogeneous Materials, *Microstructure and Macroscopic properties*, Springer-Verlag, 2002.

71. S. TORQUATO and B. LU, Chord-length distribution function for two-phase random media, *Physical Review A*, Vol.45, No.4, pp.2950-2953, 1993.

72. E.E. UNDERWOOD, *Quantitative Stereology*, Addison-Wesley, 1969.

73. E.R. WEIBEL, *Stereological Methods: Theoretical Foundations*, Vol.2, Academic Press, London, 1980.